PAPER

Check for updates

Unveiling the impact of the mpg-C₃N₄@Pa@Ni nanocomposite in the reduction of nitroaromatic derivatives by comparative solvent-free methods†

Fatemeh Eshrati, Hossein Ghafuri, ID * Peyman Hanifehnejad and Haniyeh Dogari

In this research, the impact of the mesoporous graphitic carbon nitride–papain–nickel (mpg-C₃N₄@Pa@Ni) nanocomposite in the reduction of hazardous nitroaromatic derivatives was investigated under solvent-less and solvent-free conditions. The mpg-C₃N₄@Pa@Ni composite was synthesized in four steps; synthesizing bulk and mesoporous g-C₃N₄, and functionalization with 1,3-dibromopropane, papain, and Ni nanoparticles. Papain was found to be a suitable composite material due to its ability to form covalent and coordination bonds with the substrate and Ni. Several solvent-free and solvent-less methods, including using mortar and pestle, ball mill, microwave, and magnetic stirrer, were employed to investigate the reduction of nitroaromatic compounds due to their fast, simple, and economical green nature. The synthesized nanocomposite demonstrated high efficiency rates in reducing toxic nitroaromatic compounds ranging from 80–98.6%. Structural confirmation of the mpg-C₃N₄@Pa@Ni nanocomposite was carried out using various techniques such as Fourier-Transform Infrared spectroscopy (FT-IR), N₂ adsorption analysis (BET), Field Emission Scanning Electron Microscopy (FE-SEM), Energy-dispersive X-ray spectroscopy (EDS), X-ray Diffraction spectroscopy (XRD), and Thermogravimetric Analysis (TGA). Furthermore, the mpg-C₃N₄@Pa@Ni nanocomposite showed promising recoverability without significant decreases in efficiency for up to eight cycles, indicating its potential as a sustainable and efficient catalyst. The synthesis of mpg-C₃N₄@Pa@Ni nanocomposite and its efficient performance in reducing hazardous nitroaromatic compounds pave the way for a sustainable and environmentally friendly alternative to traditional methods.

1. Introduction

Recently, carbon-based nanomaterials, including graphene, carbon nanotubes, and g-C₃N₄, have been applied in various scientific fields, including disinfection, supercapacitor, carbon dioxide reduction, degradation of pollutants, and catalysis.[1,2]

Based on the reported literature, g-C₃N₄ has superior advantages in terms of tunable band gap, abundant and low-cost precursors, biocompatibility, and structural versatility.[3–8] Pristine g-C₃N₄ has a low surface area and limited applications, while its other morphologies can broadly cover these limitations.[9] mpg-C₃N₄ has advantages over pristine g-C₃N₄ in terms of surface area, tunable pore size, chemical stability, and catalytic selectivity.[10,11] In addition, by compositing mpg-C₃N₄, its properties can be improved to a great extent.[12] Enzymes are

biocatalysts that offer high specificity and efficiency in catalyzing reactions, making them valuable components for composite material development.[13] Integrating enzymes with substrates like g-C₃N₄ can enhance catalytic activity, stability, and functionality, opening up different application opportunities in various fields.[3] Papain, a proteolytic enzyme derived from papaya, exhibits unique properties that make it an attractive candidate for composite formation with g-C₃N₄.[14] So far, much research has been published on the applications of g-C₃N₄ composites. Li *et al.* utilized graphene oxide (GO) to enhance the interfacial conductivity of g-C₃N₄, leading to the construction of a 3D porous g-C₃N₄/GO (p-CNG) framework through a template-assisted thermal treatment process.

Moreover, as electron acceptors, precious metal (Au, Pd, Pt) co-catalysts were individually anchored onto the 3D p-CNG framework to enhance active site density and facilitate electron–hole separation. Then, they tested its ability in the hydrogen evolution reaction and reported its activity to be 2565.81 μmol g⁻¹ h⁻¹ at pH = 10.5.[15] Gao *et al.* prepared a CoNiSx-g-C₃N₄ composite catalyst through a straightforward hydrothermal method. Then, they applied it in CO₂ reduction

Catalysts and Organic Synthesis Research Laboratory, Department of Chemistry, Iran University of Science and Technology, 16846-13114 Tehran, Iran. E-mail: ghafuri@iust.ac.ir

with methane and carbon monoxide production rates of 0.904 and 11.77 μmol, respectively. g-C_3N_4 composites are being explored to address various challenges that still require significant improvements. One of the global challenges today is water pollution by chemical industries.[16] Chemical industries often cause pollution by releasing harmful substances such as dyes, hazardous by-products, volatile organic compounds (VOCs), and air-suspended particles.[17,18] Nitroaromatic compounds have been widely utilized in pesticides, producing explosives, dyes, perfumes, pigments, industrial fabrication of pharmaceuticals, and insecticides.[19–22] Based on the information provided, the yearly output of nitroaromatic compounds exceeds 225000 metric tons, and approximately 9000 metric tons of this substance are released into water sources yearly.[23] The United States Environmental Protection Agency has classified nitrobenzene (simplest nitroaromatic) as a priority contaminant and has set maximum allowable concentrations of 1 mg L^{-1} and 17 μg L^{-1} in wastewater and drinking water, respectively.[24] The choice of the most effective method for removing nitroaromatic compounds, such as reduction, adsorption, advanced oxidation, or biodegradation, depends on various factors, including the specific properties of the contaminants, the desired treatment outcomes, and the efficiency and feasibility of the treatment process.[25]

While each method has advantages and limitations, reduction methods can offer fast reaction rates, potential for regeneration, and selective removal.[26–28] When nitroaromatic compounds are selectively reduced, they become amino aromatic derivatives that are more biodegradable, less toxic, and can be used as crucial synthetic intermediates in commercial processes.[29]

Metal-catalyzed reduction reactions may benefit from the cooperative interactions between metals and g-C_3N_4, enhancing catalytic performance and selectivity.[30] Pd, Ag, Cu, and Ni are the metals used with various substrates for nitroaromatic reduction reactions, including GO, MOFs, and mesoporous carbons.[31] For instance, Amit Saha *et al.* have asserted that the chemoselective reduction of nitroaromatic compounds to the corresponding amino derivatives has been achieved by combining Cu nanoparticles and ammonium formate in ethylene glycol as a solvent.[32] Moreover, the reaction yield was in the range of 75–90% at 120 °C in 8–12 h. Sean M. Kelly *et al.* have succeeded in reducing nitroaromatic compounds with zinc dust as a catalyst in the presence of water solvent at room temperature, with the best efficiency of 99% in 4 h.[33] Despite the innumerable efforts to design the optimal conditions for removing and reducing nitroaromatic compounds, these methods have limitations, such as equal solvent amount, solvent toxicity, high temperature, and long reaction time.[34] Thus, clean and efficient methods for reducing nitroaromatic compounds must be selected.[35] Mechanochemical methods are a set of techniques that involve the use of mechanical force to induce chemical reactions.[36–38] Unlike traditional chemical synthesis methods that rely on heat and solvents, mechanochemical methods utilize mechanical energy to drive reactions.[39]

In this research, we carried out a comprehensive study involving the synthesis and identification of the mpg-C_3N_4@Pa@Ni nanocomposite. Our primary objective was to investigate the catalytic performance of this nanocomposite in reducing nitroaromatic compounds using solvent-free and solvent-less methods, including using mortar and pestle, ball mill, microwave, and magnetic stirrer.[40–42] Through experiments, we identified that the magnetic stirrer method had the lowest energy consumption due to its short reaction time, environmentally friendly nature, high yield, and minimal solvent usage. Moreover, we observed an extraordinary recovery of the nanocomposite after eight reaction cycles in the magnetic stirrer method, indicating its remarkable performance in this reaction. One of the key challenges in the field of catalyst design for the reduction of nitroaromatic derivatives is the identification and optimization of active sites that can efficiently drive the reduction process. In the case of the mpg-C_3N_4@Pa@Ni nanocomposite, the active site responsible for the reduction of nitroaromatic derivatives is primarily the Ni nanoparticles. These nanoparticles provide the necessary surface for the adsorption of nitroaromatic compounds and facilitate the electron transfer required for their reduction.

Compared to other reported catalysts, the mpg-C_3N_4@Pa@Ni nanocomposite offers significant advantages. It achieves high efficiency (up to 98.6%) in significantly shorter reaction times and under mild conditions. Additionally, this catalyst demonstrates excellent recyclability, maintaining its catalytic activity after multiple cycles without a significant loss in efficiency. Furthermore, the solvent-free nature of the reduction process adheres to green chemistry principles, making this nanocomposite a more sustainable and environmentally friendly alternative to conventional methods. Overall, our research provides valuable insights into the synthesis and properties of the mpg-C_3N_4@Pa@Ni nanocomposite, highlighting its potential applications in catalytic reactions. This study not only addresses the challenge of designing efficient catalysts for nitroaromatic reduction but also demonstrates the advantages of mpg-C_3N_4@Pa@Ni as a high-performance, recyclable, and green catalyst.

2. Experimental

2.1. Materials

Phosphoric acid (95%), sulfuric acid (96%), hydrazine hydrate (98%), and other solvents and materials were purchased from Sigma-Aldrich and Merk Companies. FT-IR, FE-SEM, EDS, XRD, TGA, BET, NMR spectroscopy, and melting point analyses were carried out utilizing a Tensor 27, TESCAN-MIRA III, Numerix DXP–X10P, Dron-8 diffractometer, STA504, micromeritics ASAP 2020, VARIAN Inova 500 MHz, and Electrothermal 9100, respectively. Moreover, an Elma ultrasonic bath (80 kHz) was utilized for sonication. In addition, a Retsch Ball-mill apparatus was used with a 20 mL iron cell and two 12 mm diameter iron balls, operating at a frequency of 20 Hz. Additionally, a national

model NN-6653 microwave with a maximum power output of 900 W was also utilized.

2.2. Preparation of mesoporous graphitic carbon nitride (mpg-C$_3$N$_4$)

10 g melamine was heated in a furnace at 550 °C for 4 h to obtain bulk g-C$_3$N$_4$. Then, 2 g obtained bulk g-C$_3$N$_4$ was mixed with 20 mL sulfuric acid and 20 mL phosphoric acid in a 600 mL beaker, for 5 h at 90 °C. Subsequently, 100 mL ethanol was added to the mixture and stirred at 25 °C. After 2 h, the beaker was placed overnight at 25 °C until the precipitate settles well. In the next step, solvent spilled over, and then the resulting mixture was sonicated for 7 h to obtain the desired morphology and improve the catalyst's efficiency. Eventually, the mpg-C$_3$N$_4$ powder was obtained by separation, washing with deionized water (DW) and ethanol (1:1) by centrifugation, and drying at 60 °C.[43] A schematic for the preparation of mpg-C$_3$N$_4$ is shown in Fig. 1.

2.3. Preparation of mpg-C$_3$N$_4$@Pr–Br

In a round-bottom flask (50 mL), 1 g mpg-C$_3$N$_4$ was sonicated with 40 mL dry toluene for 1 h. Next, 2 mL 1,3-dibromopropane and 0.163 g potassium iodide (KI) were added to the previous mixture and refluxed for 24 h under N$_2$ atmosphere. Subsequently, the obtained precipitate was separated by centrifugation and washed several times with ethanol:ethyl acetate (2:1) to remove unreacted 1,3-dibromopropane. In the last step, the final product was dried at 60 °C to obtain mpg-C$_3$N$_4$@Pr–Br powder. A schematic of mpg-C$_3$N$_4$@Pr–Br is illustrated in Fig. 2.

2.4. Preparation of mpg-C$_3$N$_4$@papain

1 g mpg-C$_3$N$_4$@Pr–Br was dissolved in 3 mL dry toluene for 30 min. Thereafter, 1.6 g KI and 0.83 g papain were added to the mixture and refluxed for 12 h. Ultimately, the final product was separated, washed several times with DW:methanol (1:1), and dried at 60 °C. A schematic of mpg-C$_3$N$_4$@Pr@papain is depicted in Fig. 3.

2.5. Preparation of mpg-C$_3$N$_4$@Pa@Ni

0.5 g NiCl$_2$ was poured into a round-bottom flask (25 mL) containing 20 mL DW and stirred until it was completely dissolved. Then, 0.2 g mpg-C$_3$N$_4$@papain was added to the mixture and sonicated for 3 h. Moreover, 5 mL hydrazine hydrate and 2 mL sodium hydroxide (1 M) were added to the mixture and vigorously stirred for 3 h at 60 °C. Finally, mpg-C$_3$N$_4$@Pa@Ni was obtained by centrifugation, washed with DW:ethanol (1:1), and dried at 60 °C. A schematic of mpg-C$_3$N$_4$@Pa@Ni is shown in Fig. 4.

2.6. Reduction of nitroaromatic compounds catalyzed by mpg-C$_3$N$_4$@Pa@Ni nanocomposite

Nitroaromatic derivatives (0.125 mmol), sodium borohydride (NaBH$_4$) (1 mmol), mpg-C$_3$N$_4$@Pa@Ni (10 mg), and water as a solvent (5 μL) were added to a 25 mL round-bottom flask at room temperature. After 2 min, upon completion of the reaction (monitored by thin layer chromatography (TLC)), the catalyst was separated using a centrifuge. Then, the final product was purified via recrystallization.
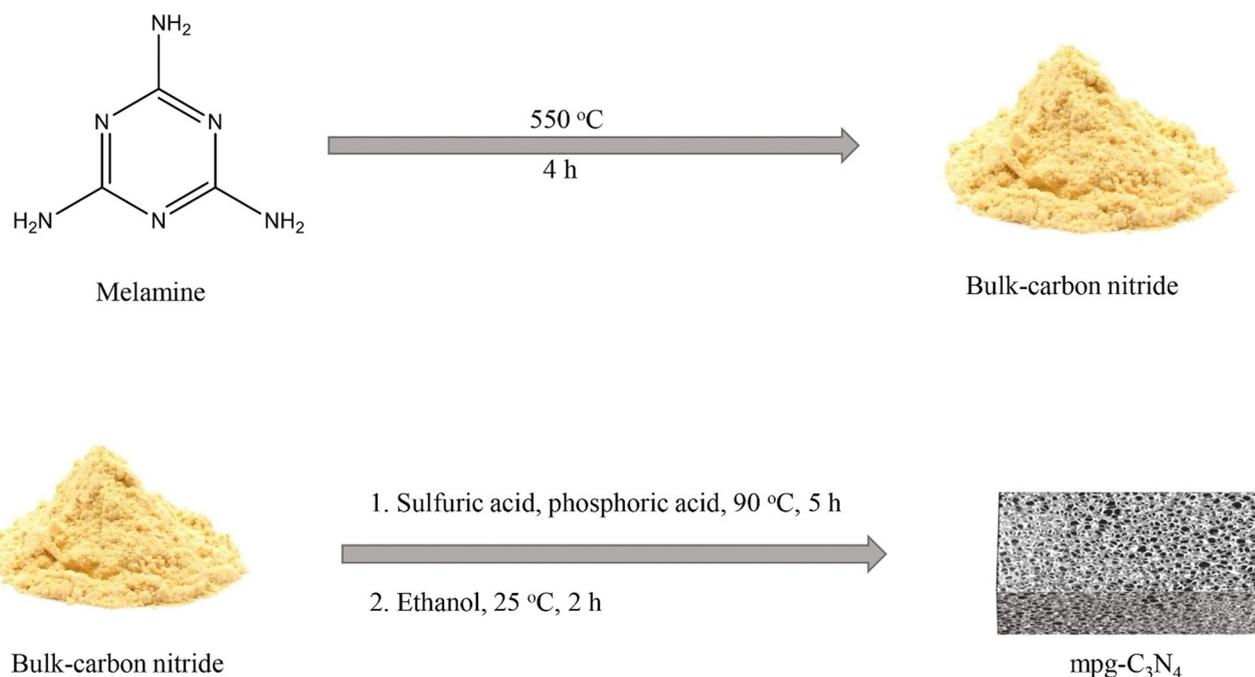

Fig. 1 The schematic preparation of mpg-C$_3$N$_4$.
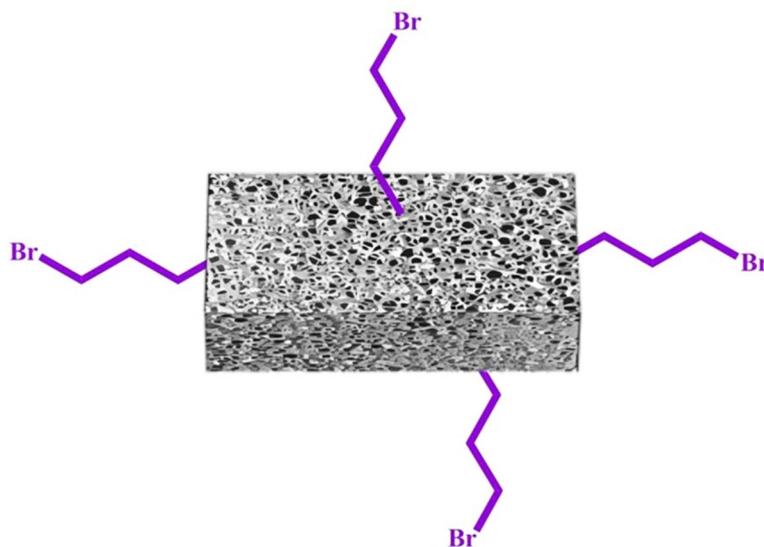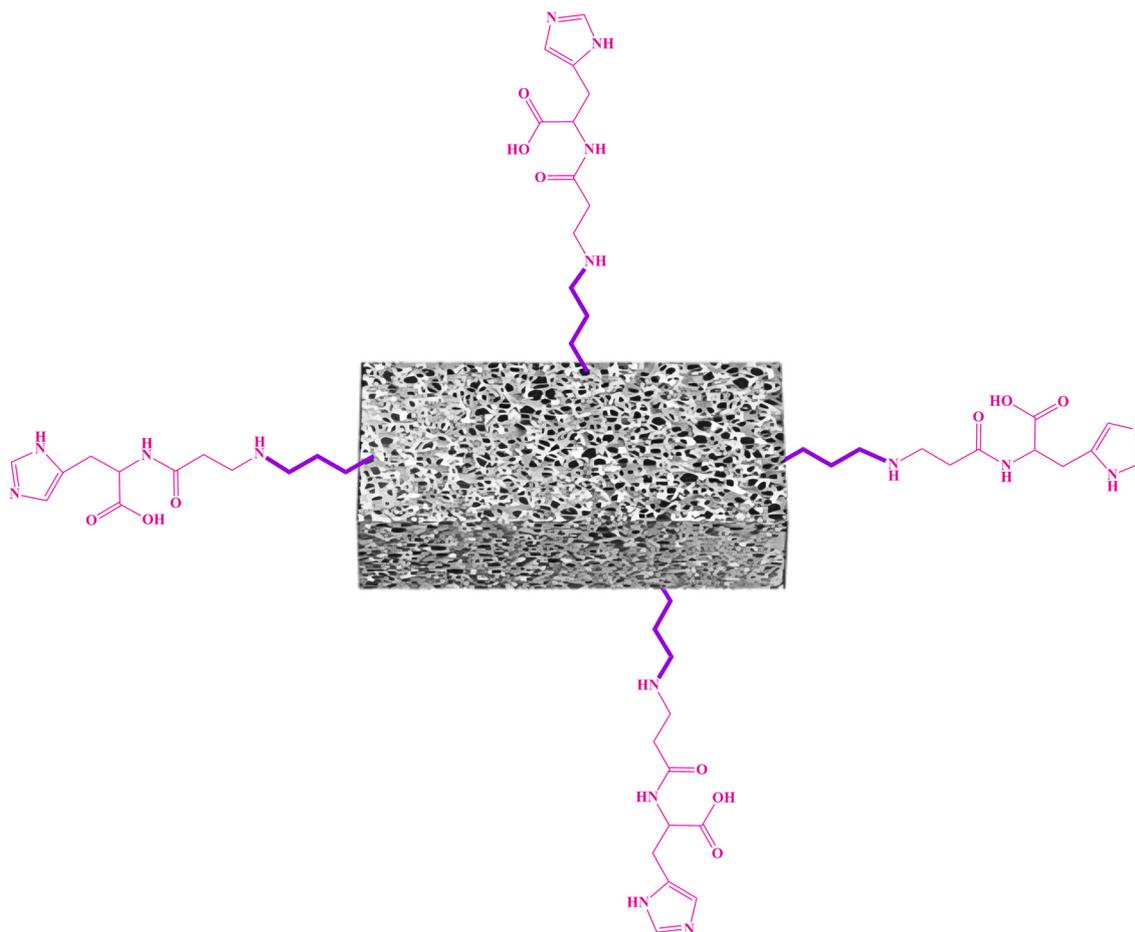
Fig. 2   Schematic of mpg-C_3N_4@Pr–Br.

Fig. 3   Schematic of mpg-C_3N_4@Pr@papain.

2.7.   Selected spectra data

2.7.1.   2-Aminobenzophenone (Table 8, entry 4). IR (KBr) $\tilde{\nu}$: 3435, 3318, 3054, 2925, 1628, 1587, 1553, 1479, 1448, 1328, 1303, 1250, 1150, 1025, 937, 911, 745, 702, 645 cm^{-1}. ^{1}H-NMR (400 MHz, DMSO) δ = 7.56 (m, 3H), 7.50 (m, 2H), 7.28 (t, 2H), 7.14 (s, 2H), 6.88 (d, 1H), 6.50 (t, 1H). NMR and
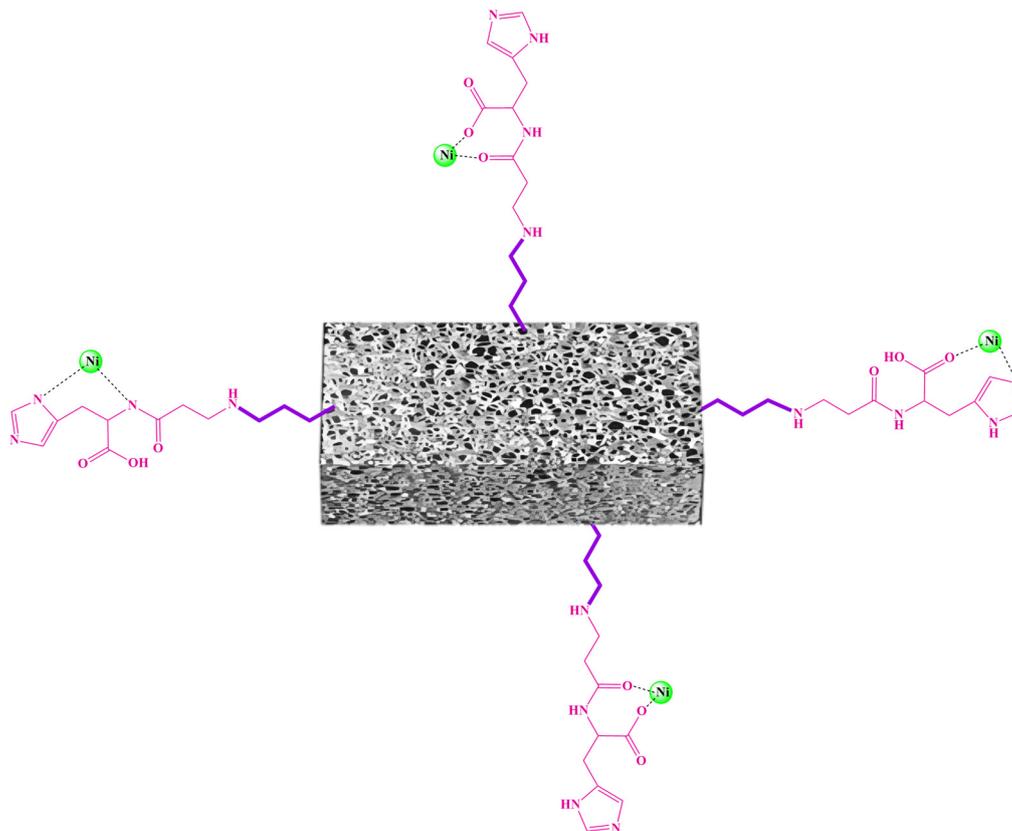
Fig. 4 Schematic of mpg-C_3N_4@Pa@Ni.

FT-IR images of 2-aminobenzophenone are shown in Fig. S3 and S4 in the ESI.†

2.7.2. 1-(4-Aminophenyl)ethanone (Table 8, entry 8). IR (KBr) $\tilde{v}$: 3398, 3331, 3221, 1652, 1590, 1361, 1305, 1282, 1178, 1134, 1071, 959, 837, 819, 597, 566, 502, 477 cm^{-1}. ^{1}H-NMR (300 MHz, DMSO) δ = 7.67 (d, 2H; ArH), 6.56 (d, 2H; ArH), 6.03 (brs, 2H; NH$_2$), 2.35 (s, 3H; CH$_3$) (Fig. S5 and S6, ESI†).

2.7.3. 4-Bromoaniline (Table 8, entry 17). IR (KBr) $\tilde{v}$: 3472, 3383, 1612, 1490, 1287, 1180, 1070, 1004, 819, 691 and 604 cm^{-1}. ^{1}H-NMR (400 MHz, DMSO): δ (ppm) 5.21–5.25 (br, 2H), 6.53–6.55 (d, 2H), 7.12–7.14 (d, 2H) (Fig. S7 and S8, ESI†).

3. Results and discussion

3.1. mpg-C_3N_4@Pa@Ni nanocomposite characterizations

To characterize the mpg-C_3N_4@Pa@Ni functional groups in each synthesis step, FT-IR analysis was taken from mpg-C_3N_4 (Fig. 5a), mpg-C_3N_4@Pr–Br (Fig. 5b), papain (Fig. 5c), mpg-C_3N_4@Pr@papain (Fig. 5d), and mpg-C_3N_4@Pa@Ni (Fig. 5e). Fig. 5a shows a wide peak around 3100–3400 cm^{-1} which may be related to the stretching vibration of –NH$_2$, –NH, groups of carbon nitride, and OH groups of adsorbed solvent. In addition, the peaks appearing around 1620, 1323, and 795 cm^{-1} are due to the stretching vibration of C=N, C–N, and triazine groups in mpg-C_3N_4. Moreover, in Fig. 5b, the peak around 2776 cm^{-1} is related to the stretching vibration of the C–H

groups associated with the presence of the 1,3-dibromopropane linker in the nanocomposite structure. Furthermore, in Fig. 5c, the broad peak around 3288–3540 cm^{-1} is related to the stretching vibration of –OH and N–H groups can be observed. Also, the peak around 2800–2967 cm^{-1} is related to the stretching vibration of the C–H groups. Furthermore, the peaks around 1651 and 1550 cm^{-1} are attributed to C=O stretching vibrations of amides and acids, which are related to papain. Besides, in Fig. 5d, all the peaks related to the previous steps are observed, which confirms the nanocomposite synthesis up to this step. Finally, in Fig. 5e, it was observed that no specific peak was detected for nickel, which may be due to its low loading in the nanocomposite.

FT-IR spectroscopy is a commonly used analytical technique in chemistry that helps identify functional groups in a given sample. However, due to its inherent limitations, it was impossible to confirm the presence of nickel particles in the final nanocomposite. In order to confirm the presence of mpg-C_3N_4@Pa@Ni elements in each step of the synthesis process, EDS analysis was performed on the final nanocomposite (as shown in Fig. 6). The EDS analysis confirmed that the first step in the synthesis process had yielded mpg-C_3N_4, as evidenced by the presence of carbon and nitrogen elements. The second step, which involved the addition of papain, was also evident from the appearance of oxygen elements. Finally, the presence of nickel element indicated the successful composition of Ni nanoparticles in the final step of mpg-C_3N_4@Pr@papain
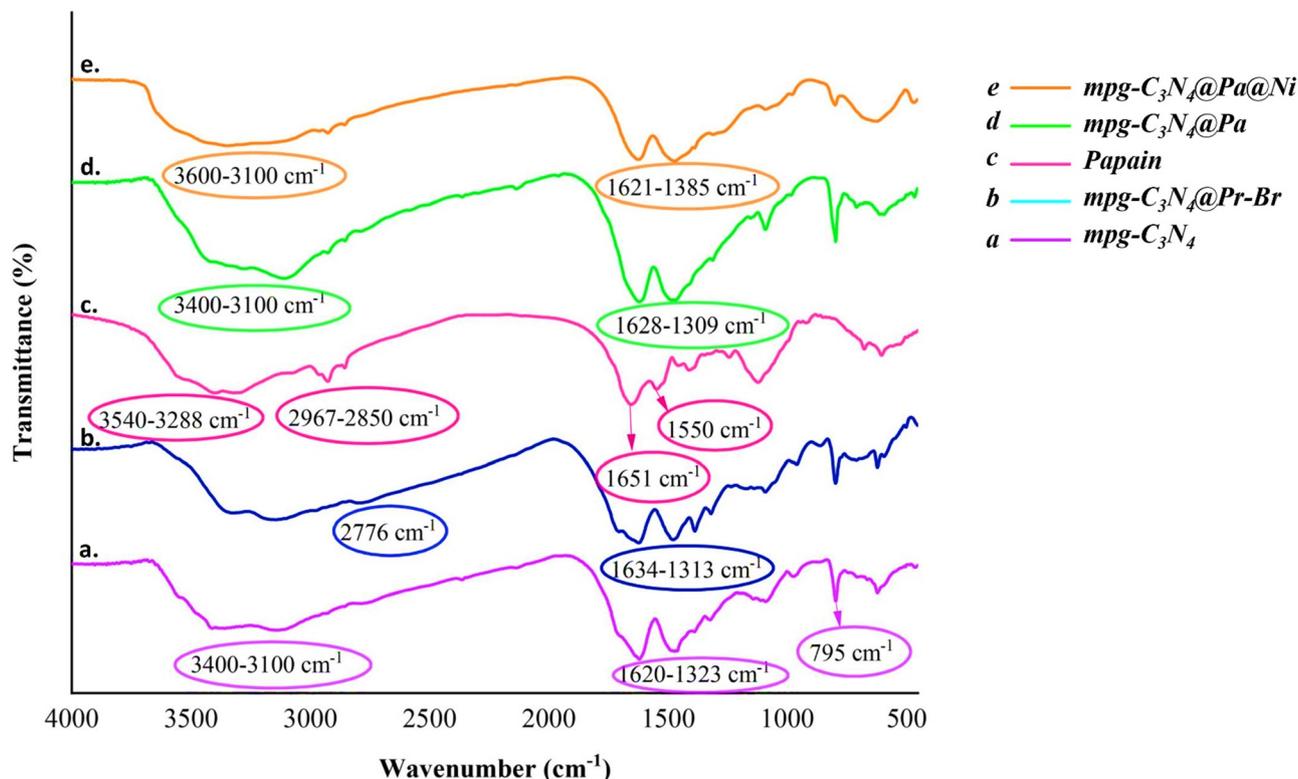
Fig. 5 The FT-IR spectra of (a) mpg-C_3N_4, (b) mpg-C_3N_4@Pr–Br, (c) papain, (d) mpg-C_3N_4@papain and (e) mpg-C_3N_4@Pa@Ni.

nanocomposite synthesis. Thus, the results of the EDS analysis provide conclusive evidence that the desired nanocomposite has been synthesized accurately in a step-by-step fashion.

The synthesized nanocomposite of mpg-C_3N_4@Pa@Ni has undergone crystallographic analysis using wide-angle XRD spectra ranging from $10°$ to $80°$ to determine its structure and composition. The results of this analysis are presented in Fig. 7. The XRD pattern of mpg-C_3N_4 was referenced to previous literature.[44] Upon analyzing the diffractograms of the nanocomposite, it was observed that distinctive peaks were present at 2θ values of $13.05°$ and $26.87°$. These peaks were attributed to the mpg-C_3N_4, which confirmed its presence in the composite material.[45] Additionally, peaks at 2θ values of $13.05°$, $19.98°$, and $38.02°$ were observed, indicating papain's presence in the structure. According to the published literature, the presence of nickel nanoparticles in the final nanocomposite structure was confirmed by peaks at 2θ values of $41.56°$, $49.91°$, and $77.34°$.[46] The improved crystallinity of the Ni nanoparticles on the mpg-C_3N_4 substrate suggests that they have been effectively composited with the mpg-C_3N_4. Therefore, it can be concluded that the synthesis of Ni nanoparticles on the mpg-C_3N_4 substrate with modifications has resulted in a successful fabrication of mpg-C_3N_4@Pa@Ni nanocomposite with improved crystallinity.

The morphological images of mpg-C_3N_4@Pa@Ni nanocomposite were examined using FE-SEM to understand its structural characteristics (Fig. 8). The FE-SEM images in Fig. 8a and b display the synthetic porous carbon nitride substrate, which confirms the porosity of the structure. The porous substrate has

numerous cavities, as evident from the images. As seen in Fig. 8c and d, the mpg-C_3N_4 surface becomes rough after being modified and through the composition with papain and nickel nanoparticles. The final nanocomposite displays an intricate network of cavities and materials, revealing the potential applications of mpg-C_3N_4@Pa@Ni nanocomposites in various fields.

The mesoporous nature of the mpg-C_3N_4@Pa@Ni nanocomposite is confirmed through both BET (Fig. 9) and pore volume distribution analysis (Fig. 10). The pore volume distribution reveals two prominent peaks in the ranges of 40–50 Å and 100–200 Å, indicating the predominance of mesopores within the material. These peaks suggest a highly concentrated distribution of mesoporous structures, contributing to a high surface area and optimal accessibility for surface reactions. The first peak, around 40–50 Å, represents smaller mesopores, while the second peak, in the range of 100–200 Å, indicates the presence of larger mesopores. The gradual decrease in pore volume beyond 200 Å suggests that the nanocomposite is primarily composed of mesoporous structures, with fewer larger pores.

Further confirmation of the mesoporous structure comes from the BET analysis, which determined the surface area and average pore size of the mpg-C_3N_4@Pa@Ni nanocomposite. As shown in Table 1, the BET surface area of the synthesized mpg-C_3N_4 is 85.9976 $m^2 g^{-1}$, with an average pore size of 24.8 nm. In comparison, literature values for g-C_3N_4 typically range from 24.1 to 59.4 $m^2 g^{-1}$, indicating that the synthesized version exhibits a significantly higher surface area, suggesting a more

Elt	A%	W%
C	38.63	35.06
N	33.26	31.89
O	21.82	23.90
Ni	6.29	9.15
	100	100
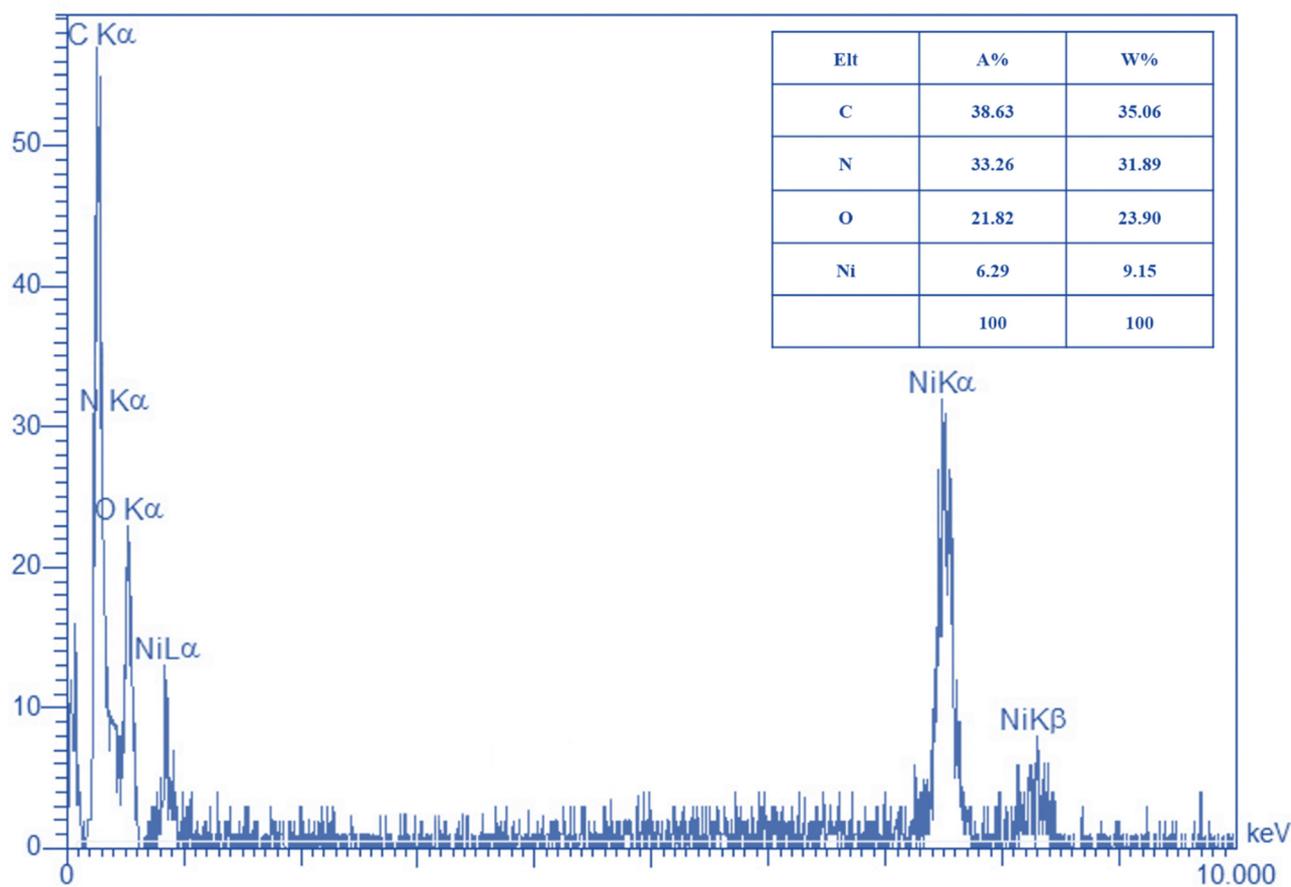
Fig. 6 The EDS spectrum of mpg-C_3N_4@Pa@Ni.

Fig. 7 The XRD pattern of mpg-C_3N_4@Pa@Ni.

© 2025 The Author(s). Published by the Royal Society of Chemistry
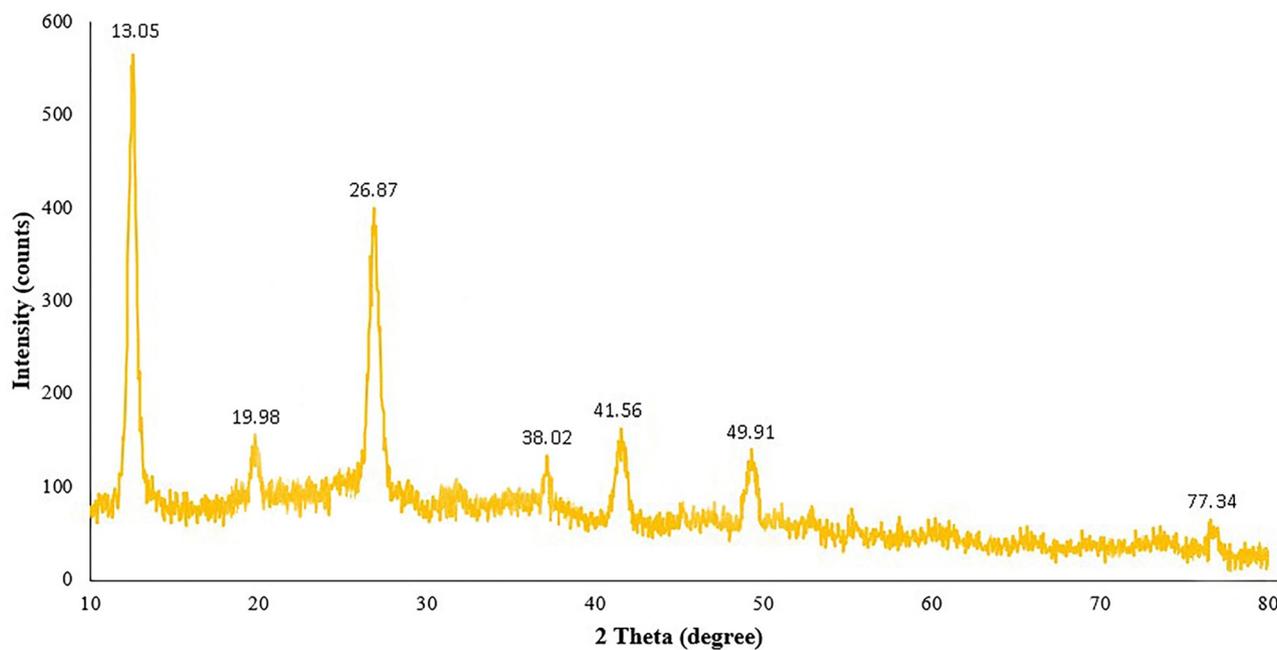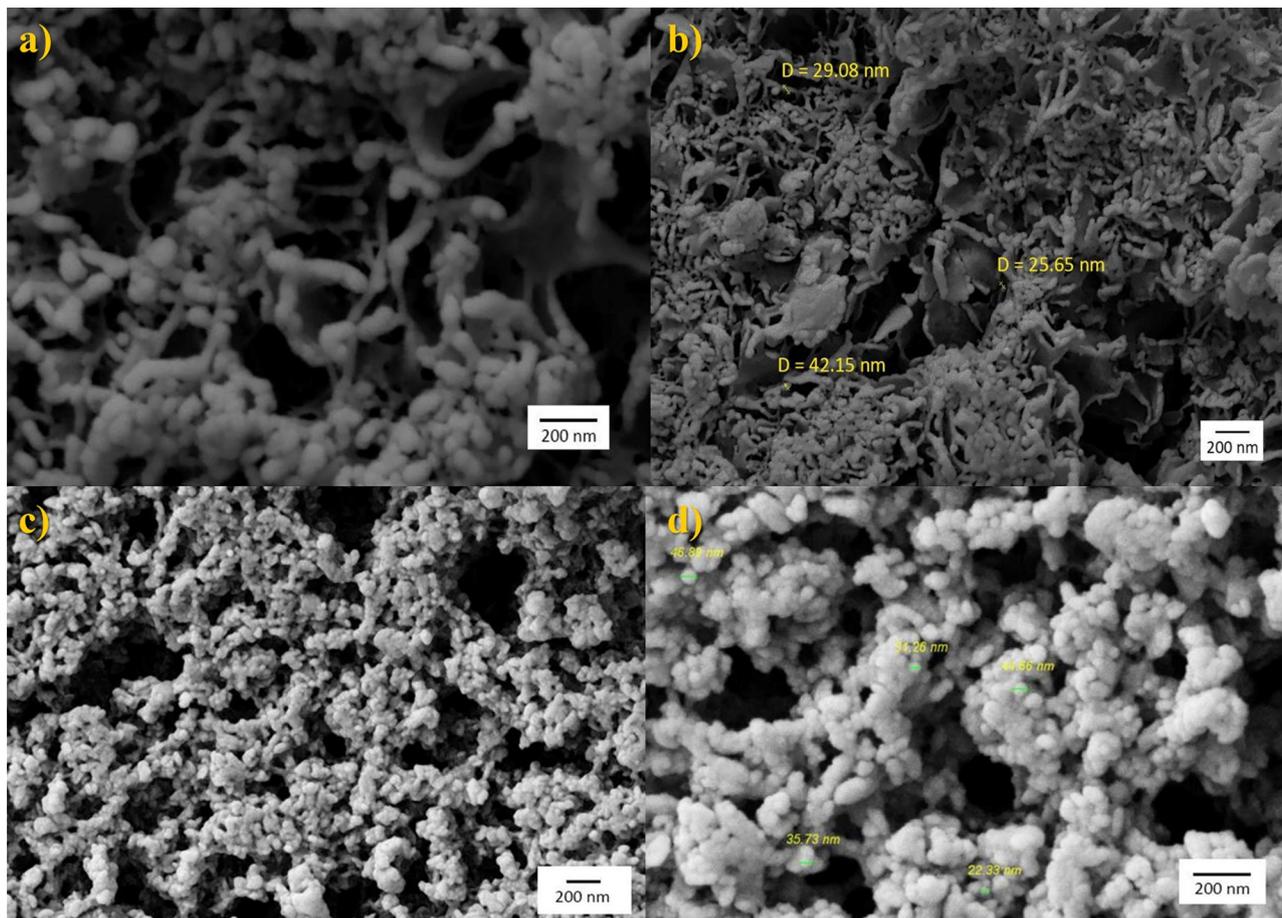
Fig. 8 FE-SEM images of (a) and (b) mpg-C_3N_4 and (c) and (d) mpg-C_3N_4@Pa@Ni nanocomposite.

porous morphology. This increase in surface area, attributed to the augmentation of the mesoporous surface area, is critical for enhancing the material's functionality.

For the final mpg-C_3N_4@Pa@Ni nanocomposite, the BET surface area increased further to 98.9716 m^2 g^{-1}, though the average pore size decreased to 15.5 nm. This reduction in pore size is expected during the integration of additional components into the mesoporous substrate, a common occurrence in nanocomposite synthesis. However, this reduction also results in the creation of new surface structures that can improve the material's properties, particularly its reactivity. The higher surface area leads to greater exposure of active sites, enabling more efficient interactions with other substances. This characteristic is especially valuable in fields such as catalysis, energy storage, and environmental remediation, where enhanced surface interactions are crucial.

Moreover, the N_2 adsorption/desorption isotherms for both mpg-C_3N_4 and mpg-C_3N_4@Pa@Ni exhibit a type (IV) adsorption isotherm, further confirming the mesoporous structure of the synthesized nanocomposite. This mesoporosity, combined with the increased surface area and new active surfaces, underscores the potential of mpg-C_3N_4@Pa@Ni for various applications.

The thermal stability of the mpg-C_3N_4@Pa@Ni nanocomposite has been thoroughly investigated using TGA analysis, as shown in Fig. 11. The TGA analysis revealed some interesting findings about the nanocomposite's thermal properties. Specifically, it was observed that the weight loss below 100 °C may be attributed to the volatilization of water or the solvent absorbed by the synthesized nanocomposite. Additionally, the weight loss observed between 225 °C and 285 °C would be credited to the thermal decomposition of papain. Moreover, the weight loss observed between 415 °C and 530 °C is related to the destruction of the structure of the mpg-C_3N_4 substrate. It is noteworthy that the remaining weight of the nanocomposite structure, which has not been destroyed up to 800 °C, is related to nickel nanoparticles occupying the mineral part of the structure. Furthermore, TGA analysis was used to calculate the mass percentage of different components of the mpg-C_3N_4@Pa@Ni nanocomposite (see the whole calculation in the ESI†). Based on Fig. 11, the solvent present in the structure contributes to approximately 8% of the total mass. Moreover, the TGA analysis of the mpg-C_3N_4@Pa@Ni nanocomposite revealed that papain and 1,3-dibromopropane constitute 50% of the total mass, while mpg-C_3N_4 contributes 19% and nickel nanoparticles contribute 23%. This information
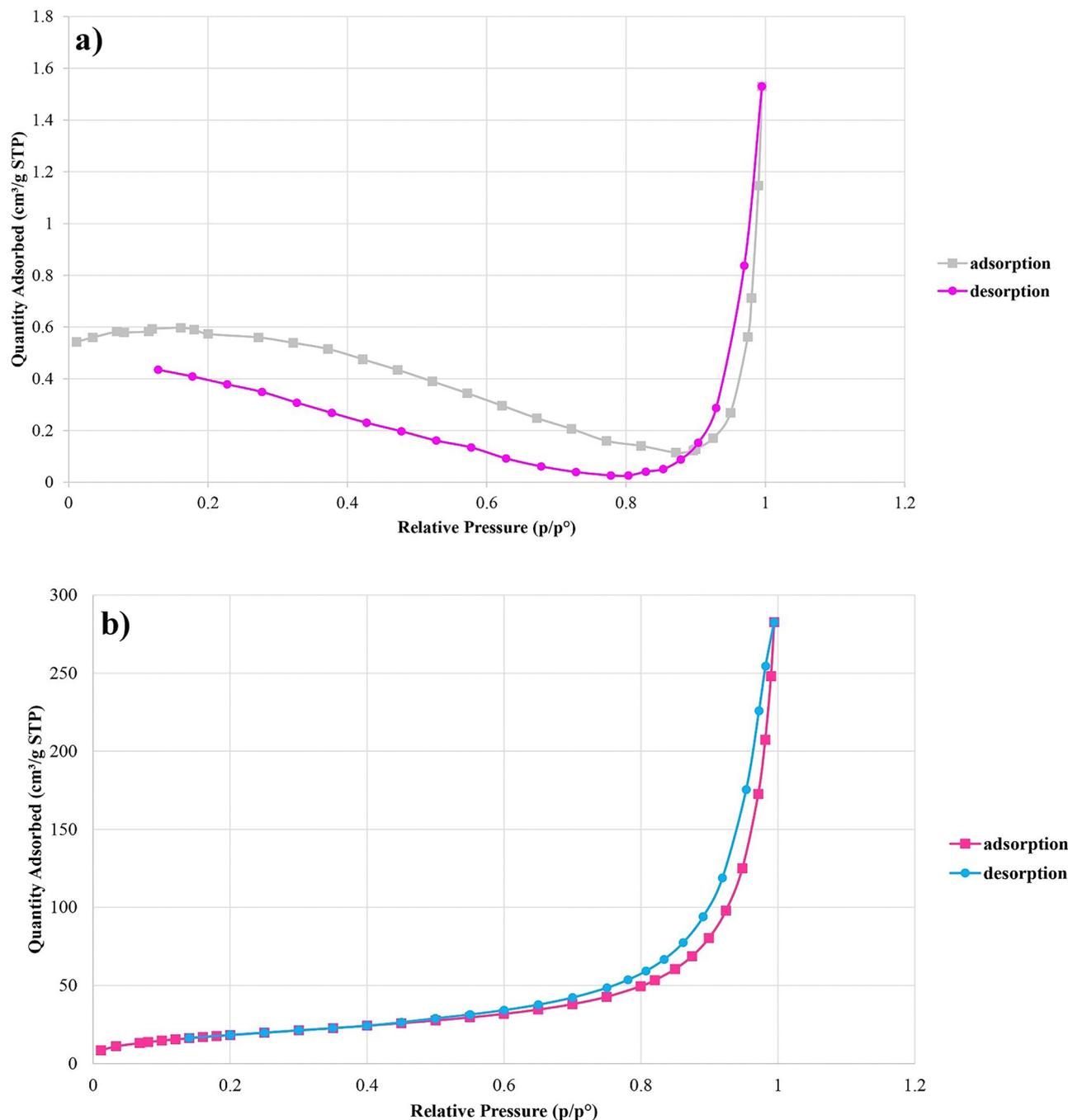
Fig. 9 Isotherm linear plots of (a) mpg-C_3N_4 and (b) mpg-C_3N_4@Pr@papain@Ni.

provides detailed insight into the composition of the unique mpg-C_3N_4@Pa@Ni nanocomposite, which has potential applications in various fields due to its remarkable thermal stability and composition.

3.2. Survey of different solvent-less methods toward nitroaromatics reduction

Reduction reactions, which involve the addition of electrons to the nitro group, are key to detoxifying nitroaromatic compounds. These reactions transform highly reactive and harmful nitro groups into less toxic amine or hydroxylamine derivatives. This conversion not only reduces the immediate toxicity of the compounds but also facilitates further degradation through microbial or abiotic processes. In this research, various parameters, such as solvent, reaction time, amount of catalyst, and reaction temperature, were investigated to optimize the reduction reaction conditions. To find the optimal reaction conditions, the reaction between
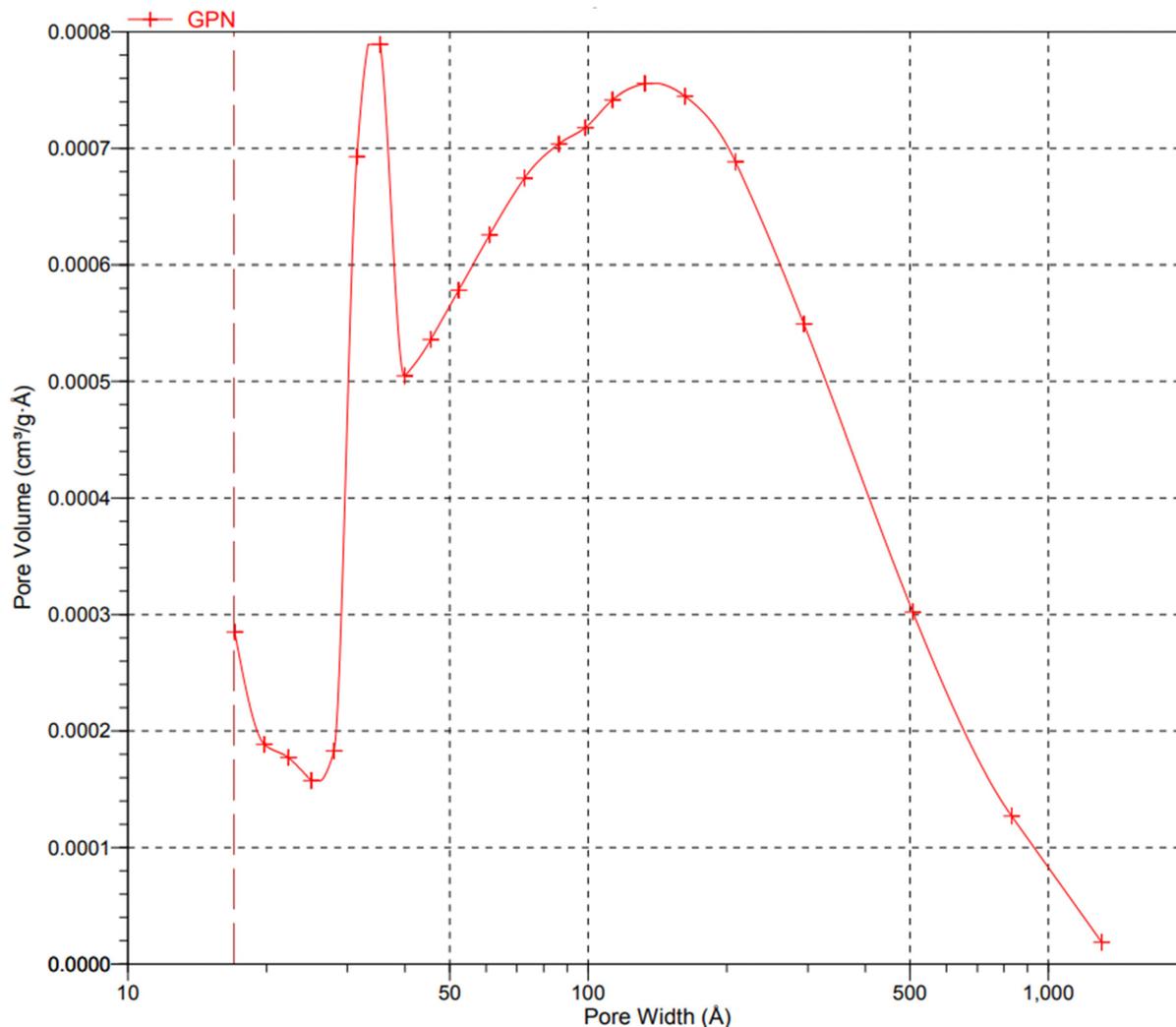
Fig. 10 Pore size distribution patterns of mpg-C$_3$N$_4$@Pa@Ni.

Table 1 Surface area, pore volume, and pore size of mpg-C$_3$N$_4$ and mpg-C$_3$N$_4$@Pa@Ni

Sample	Surface area (m^2 g^{-1})	Pore volume^a (cm^3 g^{-1})	Average size (nm)	Ref.
g-C$_3$N$_4$ nanosheet	24.1	—	—	47
g-C$_3$N$_4$ nanosheet	59.4	—	—	48
mpg-C$_3$N$_4$	85.9976	0.438832	24.8	This work
mpg-C$_3$N$_4$@Pa@Ni	98.9716	0.388148	15.5	This work

^{a} Determined at p/p^0 = 0.97, where p is the equilibrium pressure and p^0 is the saturation pressure of nitrogen at −196 °C.

4-nitrophenol (0.25 mmol) and NaBH$_4$ (1 mmol) along with mpg-C$_3$N$_4$@Pa@Ni as a catalyst (10 mg) and water as a solvent (5 μL) at 25 °C for 2 min was considered as the model reaction for reducing nitroaromatic compounds (Fig. 12). To achieve the highest possible product yield, the anti-solvent method (using a combination of ethyl acetate and n-hexane) was employed for product isolation. With these optimized conditions, the highest possible yield of the desired product was obtained.

During the initial phase of optimizing the reaction conditions, it was observed that the reaction proceeded favorably at

ambient temperature (25 °C) and in the presence of water as the solvent. To further optimize the reaction, these two parameters were kept constant. Afterward, the study aimed to explore the interaction of nitroaromatic derivatives (0.25 mmol) with sodium borohydride under various conditions and according to the principles of green chemistry. The study was performed in line with the principles of green chemistry, which emphasize the use of eco-friendly and sustainable chemical processes. These conditions included the presence or absence of catalyst and solvent. The reactions occurred at room temperature,
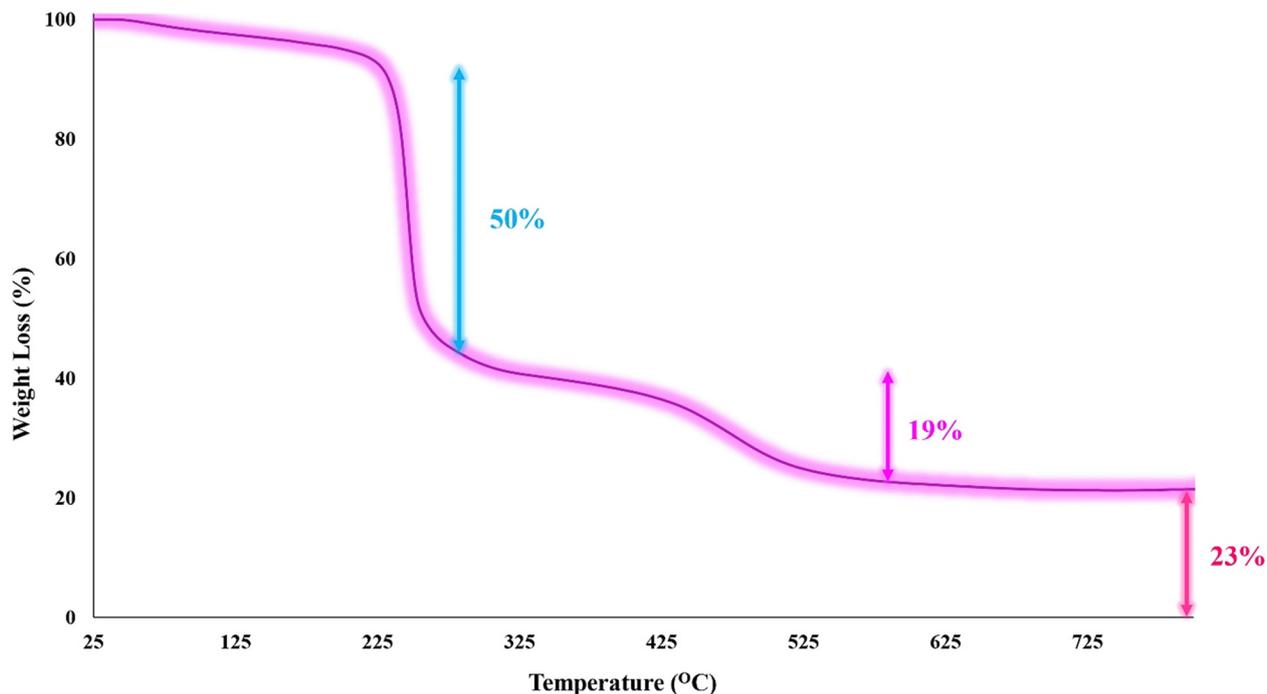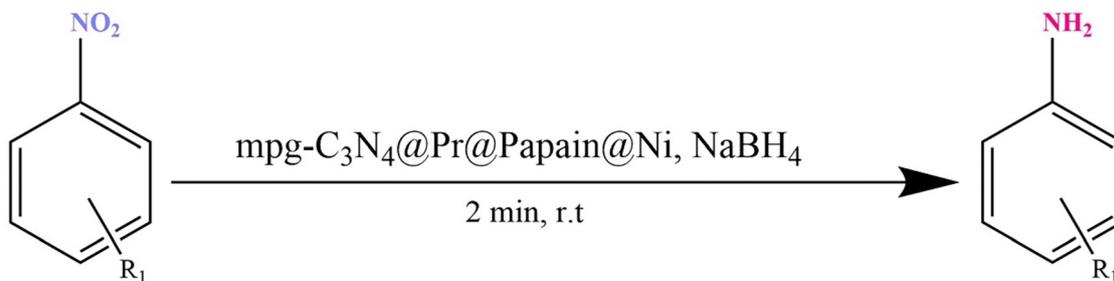
Fig. 11 The TGA pattern of mpg-C$_3$N$_4$@Pa@Ni.

Fig. 12 mpg-C$_3$N$_4$@Pa@Ni catalyzed reduction of nitroaromatic compounds.

which was set at 25 °C, using solvent-free methods such as using magnetic stirrer, microwave, ball mill, and mortar and pestle. During the study, the progress and completion of the reactions were monitored using TLC.

3.2.1. Mortar and pestle method. In the first step, optimal conditions were investigated for the mortar and pestle method (Table 2). At the onset, a reaction was performed in the absence of solvent, with 1 mmol NaBH$_4$ and 10 mg catalyst, within 5 min, and the results showed that no significant product was obtained (entry 1). Subsequently, the reaction was carried out in the presence of 5 μL water as a solvent in 3, 4, and 5 min, respectively. It was observed that by reducing the reaction time from 5 min to 3 min, the efficiency decreased from 98.6% to 48% (entries 2–4). The method boasts advantages like effective mixing, suitability for lab-scale use, affordability, and adaptability to reactions involving solid or semi-solid materials. However, some drawbacks to this method include time consumption, limited scalability, potential residual material contamination, and a lack of precision compared to solvent-free methods due to manual force. Despite the drawbacks, utilizing

Table 2 Optimizing the reaction conditions for reducing nitroaromatic compounds with the mortar and pestle method

Entry	Nitro compound (mmol)	NaBH$_4$ (mmol)	Catalyst (mg)	Solvent (μL)	Time (min)	Yield (%)
1	0.25	1	10	—	5	Trace
2	0.25	1	10	5	5	98.6
3	0.25	1	10	5	4	83
4	0.25	1	10	5	3	48

Table 3 Optimizing the reaction conditions for the reduction of nitroaromatic compounds with the ball milling method

Entry	Nitro compound (mmol)	NaBH$_4$ (mmol)	Catalyst (mg)	Solvent (μL)	Ball mill (ball)	Time (min)	Yield (%)
1	0.25	1	10	—	30 Hz (1)	5	41
2	0.25	1	10	—	30 Hz (3)	5	29
3	0.25	1	10	5	20 Hz (1)	3	70
4	0.25	1	10	5	25 Hz (1)	7	98.6
5	0.25	1	10	5	30 Hz (2)	5	98.6
6	0.25	1.5	10	5	30 Hz (2)	5	98.6
7	0.25	0.73	10	5	30 Hz (1)	5	98.6
8	0.25	1	8	5	30 Hz (1)	5	86

the mortar and pestle method in chemical reactions can have environmental benefits, such as reduced energy consumption, minimized waste, avoidance of hazardous solvents, and increased equipment longevity.

3.2.2. Ball milling method. Ball milling is a mechanical process that involves using a rotating container filled with balls to reduce the size of particles and facilitate chemical reactions. The ball milling method is superior to the mortar and pestle method for liquid-assisted grinding reactions because it allows for more efficient, homogeneous, and accurate processing. The ball mill's rotating mechanism provides better particle size reduction and mixing compared to manual grinding with a mortar and pestle. Some advantages of this method are homogeneous mixing, synthesis of nanomaterials, and high reaction rates. On the other hand, energy consumption and equipment costs are among the disadvantages of using the ball milling method. Moreover, the ball milling method offers some environmental benefits compared to traditional chemical synthesis methods like green synthesis, energy efficiency, and safer reaction conditions. In this step, optimal conditions for the ball milling method were explored (see Table 3). Various elements, such as the type of solvent, reducing agent, number of balls (stainless steel), frequency, and catalyst quantity, played a significant role in determining the reaction efficiency.

Firstly, the reaction was performed using 1 mmol NaBH$_4$ and 10 mg catalyst, in the absence of water as a solvent with one ball, achieving an efficiency of 41% (entry 1). However, when the same reaction was performed using 3 balls, the efficiency dropped to 29% (entry 2). This difference can be attributed to the use of only one ball, which reduces the number of ineffective collisions and enhances the effective ones by providing the necessary energy to initiate the reaction. In the presence of 5 μL water and 3 min reaction time, using only one ball at a frequency of 20 Hz, the efficiency was significantly improved to 70% (entry 3). Further raising the frequency to 25 Hz resulted in achieving the desired product in 7 min with 98.6% efficiency, thanks to enhanced effective collision and the provision of necessary energy to initiate the reaction (entry 4). By increasing the number of balls to 2, adjusting the frequency to 30 Hz, utilizing 1 mmol NaBH$_4$, and reducing the reaction time to 5 min, the reaction yield was attained to be 98.6% (entry 5). Comparing the results from entries 6 and 7, it is evident that while both achieved a high efficiency of 98.6%, several key reaction parameters were varied. In entry 6, two balls were used at a frequency of 30 Hz with 1.5 mmol NaBH$_4$. In contrast,

entry 7 involved the use of only one ball at a frequency of 30 Hz but with a reduced NaBH$_4$ quantity of 0.73 mmol. Despite the reduction in the amount of NaBH$_4$, the efficiency remained at 98.6%. This can be attributed to the fact that decreasing the number of balls from two to one reduces the number of ineffective collisions, allowing more efficient energy transfer and a higher proportion of effective collisions. Consequently, while the amount of reducing agent was lowered in entry 7, the optimized collision dynamics compensated for this change, maintaining the reaction efficiency. Therefore, both the number of balls and the amount of NaBH$_4$ contribute significantly to the reaction's overall performance and must be considered together when optimizing conditions. However, diminishing the catalyst amount to 8 mg resulted in an 86% decrease in reaction efficiency within 5 min (entry 8). This decline can be ascribed to the reduction in catalyst quantity, consequently diminishing the available active sites for the reduction reaction.

Conclusively, the optimal reaction conditions involved 5 μL water, 0.73 mmol NaBH$_4$, and 10 mg catalyst, using 1 ball at a frequency of 30 Hz for a duration of 5 min (entry 7). These conditions were found to be the most efficient in terms of reaction yield, time, and cost.

3.2.3. Microwave method. Microwave-assisted method have been gaining popularity for their notable benefits such as energy efficiency, selective heating, and scale-up potential. Compared to traditional ball milling, microwave-assisted reactions often demonstrate shorter reaction times, contributing to increased overall efficiency in chemical processes. Additionally, microwave methods can provide selective heating to specific reaction components, allowing for enhanced control and optimization of reactions. Despite these benefits, the microwave method presents challenges in reaction optimization and safety concerns. Nevertheless, it boasts several environmental benefits such as lower energy consumption, faster reaction rates, and reduced solvent usage.

The optimal conditions were explored in the microwave method in the presence and absence of water as a solvent, various amounts of catalyst, and NaBH$_4$ for different reaction times (see Table 4). Initially, the results showed that in the absence of water and using 1 and 1.5 mmol NaBH$_4$ in the presence of 10 mg of catalyst, and within 5 min, no significant product was obtained (entries 1 and 2). In the trial, the addition of 5 μL water to the reaction within 2 min resulted in 98.6% efficiency (entry 3). Furthermore, by reducing the reaction time

Table 4 Optimizing the reaction conditions for reducing nitroaromatic compounds with the microwave method

Entry	Nitro compound (mmol)	NaBH$_4$ (mmol)	Catalyst (mg)	Solvent (μL)	Time (min)	Yield (%)
1	0.25	1	10	—	5	Trace
2	0.25	1.5	10	—	5	Trace
3	0.25	1	10	5	2	98.6
4	0.25	1	10	5	1	42
5	0.25	0.73	10	5	2	91
6	0.25	1	8	5	2	76

to 1 min, an efficiency of 42% was obtained (entry 4). These results indicate that the reaction is incomplete in less than 2 min, and adjusting the reaction time is markedly effective in efficiency. Furthermore, the influence of NaBH$_4$ amount was examined, and it was discovered that reducing the NaBH$_4$ amount to 0.73 mmol resulted in 91% efficiency (entry 5). Thus, a marginal decrease in NaBH$_4$ quantity does not adversely impact reaction efficiency. Conversely, exploring the impact of the catalyst amount revealed that decreasing it to 8 mg led to a decline in reaction efficiency to 76% within 2 min (entry 6). This can be ascribed to the reduced catalyst amount, subsequently diminishing the active sites available for the reduction reaction. Ultimately, the best reaction conditions were identified using microwaves in the presence of water (5 μL), 1 mmol NaBH$_4$, and 10 mg of catalyst in 2 min (entry 3). These findings provide valuable insights into the optimization of microwave-assisted reactions and can be useful for further development and improvement of chemical processes.

3.2.4. Magnetic stirrer method. In solvent-free methods, a magnetic stirrer is often used to facilitate efficient mixing and dispersion of reactants, promoting homogeneity in the absence of a solvent. This method offers advantages such as uniform mixing, consistent reaction conditions, and user-friendly operation. However, it may not be suitable for high-viscosity reactions and has limited heat transfer efficiency. On the other hand, utilizing microwaves in the process has limitations due to generating harmful waves and increased temperatures during the reaction.

3.2.5. In-depth comparison of methods for nitroaromatic reduction. In this study, four different methods—mortar and pestle, ball milling, microwave, and magnetic stirrer—were applied for the reduction of nitroaromatic derivatives using the mpg-C$_3$N$_4$@Pa@Ni nanocomposite. While all methods achieved the same catalytic efficiency (98.6%), they differed significantly in terms of energy consumption, reaction time, ease of use, and scalability, which makes each method suitable for different applications.

The mortar and pestle method required the least amount of energy, as it only relied on manual force and did not need any external energy input. However, the reaction time was longer, taking 5 min to reach 98.6% efficiency. Reducing the reaction time to 3 min led to a significant drop in yield (48%), showing that consistent manual mixing is challenging for shorter reaction times. This method is suitable for small-scale laboratory experiments, where simplicity and low cost are important, but

its limited scalability and inconsistent mixing make it less ideal for larger, industrial applications.

The ball milling method provided more controlled and homogeneous mixing due to mechanical energy input. It reached 98.6% efficiency in 5 min at an optimal frequency of 30 Hz using 1 ball. While this method consumes more energy compared to using a mortar and pestle, it offers better precision and is scalable, making it suitable for both small- and large-scale applications. The mechanical agitation ensures uniform particle size reduction and consistent results, but its energy consumption is higher, which can be a limitation for energy-conscious processes.

The microwave method was the fastest, achieving 98.6% efficiency in just 2 min. Microwave heating provides selective energy transfer, accelerating the reaction kinetics. However, reducing the reaction time to 1 min drastically lowered the efficiency to 42%, which indicates that time control is critical. While microwaves are excellent for rapid reactions and energy-efficient in terms of speed, the overall energy usage can be higher compared to mechanical methods. Scaling up microwave reactors for industrial applications can also be challenging, as ensuring uniform heating across larger volumes requires specialized equipment.

The magnetic stirrer method stood out as the most energy-efficient and practical for scale-up. It achieved 98.6% efficiency in 2 min, with minimal energy consumption for stirring and very low solvent use. Additionally, the method demonstrated excellent catalyst recovery and reusability, maintaining high efficiency over eight cycles. Its simplicity, low energy requirements, and scalability make it the most suitable method for sustainable industrial-scale applications, where energy efficiency and ease of use are crucial.

In conclusion, although all methods reached similar catalytic efficiency, each method has specific advantages depending on the application. The magnetic stirrer method is ideal for large-scale, energy-efficient processes due to its low energy consumption and high performance. The ball milling method is suitable for applications requiring precise control and homogeneous mixing, though it is more energy-intensive. The microwave method excels in rapid reactions but requires careful time optimization and specialized equipment for scaling. Lastly, the mortar and pestle method, while simple and cost-effective, is best suited for small-scale, less demanding experiments where energy consumption is not a major concern.

3.2.6. Optimization of reaction conditions for maximum efficiency in nitroaromatic reduction. After conducting various

Table 5 Optimizing the reaction conditions for reducing nitroaromatic compounds with the magnetic stirrer method

Entry	Nitro compound (mmol)	NaBH$_4$ (mmol)	Catalyst (mg)	Solvent (μL)	Time (min)	Yield (%)
1	0.25	2	10	—	9	Trace
2	0.25	2	10	5	9	98.6
3	0.25	1	10	5	2	98.6
4	0.25	1.5	7	5	5	84
5	0.25	1.5	10	5	1	48
6	0.25	1.6	5	5	2	40
7	0.25	0.73	15	5	2	95

methods, the optimal conditions in the magnetic stirrer method were extensively investigated (see Table 5). Initially, the reaction was carried out without water as a solvent in the presence of 2 mmol NaBH$_4$, 10 mg catalyst, for 9 min. However, this reaction condition did not yield any significant efficiency (entry 1). To improve the efficiency of the reaction, 5 μL water was added, and an efficiency of 98.6% (entry 2) was achieved. In summary, the presence of solvent in the reduction of nitroaromatic compounds with NaBH$_4$ ensures efficient mixing, homogeneous reaction conditions, and temperature control, facilitating activation of the reducing agent, and contributing to the success of the reduction process. Further optimization was carried out to determine the optimal time and the amount of NaBH$_4$. The reaction time was reduced to 2 min, and the amount of NaBH$_4$ was decreased to 1 mmol, resulting in a 98.6% efficiency (entry 3). However, when the reaction time was reduced to 1 min, and the amount of NaBH$_4$ was increased to 1.5 mmol, the efficiency decreased to 48% due to the incomplete reaction. Thus, adjusting the reaction time is markedly effective in efficiency (entry 5).

In addition, the amount of catalyst and NaBH$_4$ was varied to determine their effect on the reaction efficiency. By reducing the amount of catalyst to 7 mg, the active sites available for the reduction reaction were diminished, resulting in 84% efficiency (entry 4). Furthermore, by reducing the catalyst to 5 mg and increasing the amount of NaBH$_4$ to 1.6 mmol, an efficiency of 40% was attained (entry 6), which can be attributed to the reduced amount of catalyst and fewer active sites for the reduction reaction. In the following, by reducing the amount of NaBH$_4$ to 0.73 mmol and increasing the catalyst to 15 mg, a 95% efficiency was achieved within 2 min (entry 7). Thus, a negligible decrease in NaBH$_4$ amount does not adversely impact reaction efficiency, and the reaction efficiency has been improved due to the increase in the amount of catalyst and, as a result, the increase in active sites. Finally, the optimal reaction conditions for the reduction of nitroaromatic compounds with NaBH$_4$ were achieved in the presence of 5 μL water, at ambient temperature, and when stirred for 2 min (entry 3). These findings highlight the importance of optimizing reaction conditions to achieve maximum efficiency and can pave the way for future studies in this field.

In addition to optimizing the reaction conditions, the composition and quantity of materials in the nanocomposite also have a significant impact on catalytic performance. The nickel (Ni) content in the mpg-C$_3$N$_4$@Pa@Ni nanocomposite is pivotal in enhancing its catalytic performance by providing essential active sites. Therefore, the effect of increasing the nickel content in the nanocomposite was investigated. Doubling the Ni loading effectively increased the number of these active sites, leading to improved electron transfer and a boost in the reduction efficiency of nitroaromatic compounds to 99%. The well-dispersed Ni nanoparticles on the mesoporous g-C$_3$N$_4$ matrix facilitated synergistic interactions, enhancing catalytic activity without causing agglomeration. This optimized Ni loading maintained high selectivity and a balanced combination of activity and stability, as shown by TGA analysis indicating that Ni also contributes to the thermal stability of the catalyst. This stability enables effective reuse over at least eight cycles with minimal performance loss. However, while the increased Ni content did enhance reduction efficiency, the marginal improvement in catalytic performance may not justify the cost of doubling the Ni nanoparticle content on the composite. Therefore, careful consideration of Ni loading is crucial for achieving both maximum catalytic efficiency and cost-effectiveness, supporting the composite's long-term reusability in sustainable catalytic applications.

After examining various solvent-free and solvent-less methods to reduce nitroaromatic derivatives, even though 98.6% efficiency was obtained in all methods, the magnetic stirrer method was selected as the optimal method due to its ease of use and the lack of high energy consumption (Table 6). By using the magnetic stirrer method, the desired products were produced with remarkable performance. This was achieved by utilizing 1 mmol NaBH$_4$, 10 mg catalyst, and 5 μL solvent, for 2 min at ambient temperature. Overall, the magnetic stirrer method proved to be a reliable and effective approach for regenerating derivatives.

Also, the reaction was performed under optimal conditions to evaluate the effect of each component on the reaction catalyst (Table 7). The first step involved using mpg-C$_3$N$_4$@Pr@Pa with NaBH$_4$ as the reducing agent. However,

Table 6 Comparison of optimized methods for the reduction of nitroaromatic compounds[a]

Entry	Method	NaBH$_4$ (mmol)	Time (min)	Yield (%)
1	Mortar and pestle	1	5	98.6
2	Ball milling (1 ball, 30 Hz)	0.73	5	98.6
3	Microwave	1	2	98.6
4	Magnetic stirrer	1	2	98.6

[a] Reaction conditions: nitroaromatic compounds (0.25 mmol), catalyst (10 mg), and solvent (5 μL), at 25 °C.

Table 7 The efficiency of mpg-C$_3$N$_4$@Pa@Ni nanocomposite with its components

| Entry	Catalyst	Yield^a (%)
1	mpg-C$_3$N$_4$@Pr@Pa, NaBH$_4$	Trace
2	mpg-C$_3$N$_4$@Pa@Ni	15
3	NaBH$_4$	30
4	Ni nanoparticle, NaBH$_4$	60
5	mpg-C$_3$N$_4$@Pa@Ni, NaBH$_4$	98.6

^{a} The yields relate to the isolated product.

the results showed a relatively low percentage of the intended product due to the limited reduction by NaBH$_4$ as a reducing agent. On the other hand, the final nanocomposite (mpg-C$_3$N$_4$@Pa@Ni) without NaBH$_4$ reduced the final product's percentage due to the lack of a proton-donating agent. Furthermore, using NaBH$_4$ alone as the auxiliary reducing agent also did not yield significant results, with the product percentage being negligible. However, when Ni nanoparticles were added to the NaBH$_4$, a more favorable percentage of 60% was observed due to the protonation of Ni by NaBH$_4$, leading to an increase in reduction efficiency. Finally, using the mpg-C$_3$N$_4$@Pa@Ni nanocomposite with NaBH$_4$ resulted in the best product percentage (98.6%) due to the favorable surface area and the presence of abundant active sites. In conclusion, the investigation results confirmed that the most effective catalyst for reducing nitroaromatic compounds is the mpg-C$_3$N$_4$@Pa@Ni nanocomposite with NaBH$_4$. This study provides valuable insights into the development of efficient catalytic systems for reducing nitroaromatic compounds in the chemical industry.

In order to exhibit the catalytic merits of mpg-C$_3$N$_4$@Pa@Ni nanocomposite, the optimized conditions were applied to nitroaromatic compounds containing electron-donating or withdrawing groups, as shown in Table 8. The study aimed to determine the effects of different electron-donating and -withdrawing groups on the reaction process. The results showed that the reaction was not significantly influenced by the presence of either electron-donating or -withdrawing groups. In fact, all the nitroaromatic compounds were reduced in high yields, as demonstrated in Table 8. These findings suggest that using the mpg-C$_3$N$_4$@Pa@Ni nanocomposite could be a promising catalyst for reducing nitroaromatic compounds, regardless of their electronic properties (Table 8).

3.3. Comparing the efficiency of mpg-C$_3$N$_4$@Pa@Ni nanocomposite with other published literature

For indicating the catalytic merits of mpg-C$_3$N$_4$@Pa@Ni nanocomposite the model reaction was compared with some other

Table 8 Reduction of nitroaromatic derivatives under the optimized conditions using mpg-C$_3$N$_4$@Pa@Ni^a
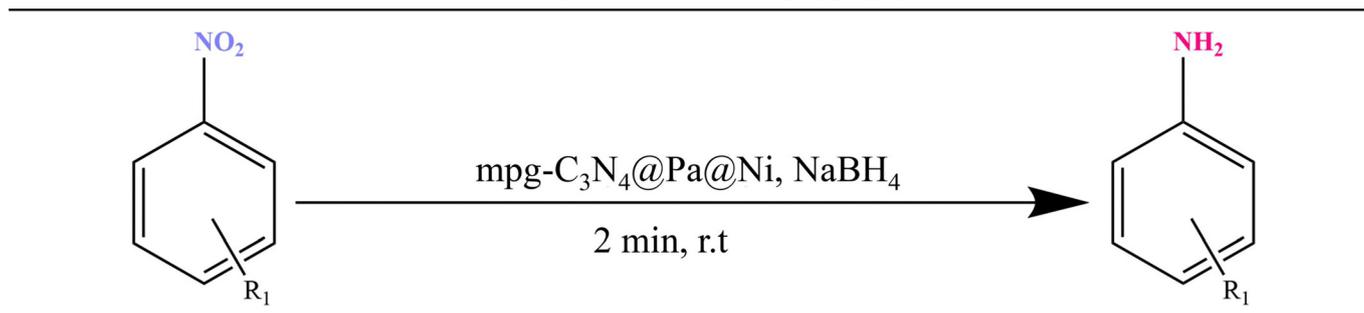
Entry	R$_1$	Yield^b (%)	M.P. (°C) Found	M.P. (°C) Reported (ref.)
1	H	98.6	Liquid sample	
2	3-NO$_2$	97.4	64–66	65–66 (49)
3	2-NO$_2$	97.2	99–103	100–102 (50)
4	2-COPh	98.4	106–107	105–107 (51)
5	4-OH	98.6	186–189	187–189 (52)
6	4-CH$_2$OH	97.4	62–64	60–65 (50)
7	3-CHO	98	28–31	29–32 (53)
8	4-COMe	97.6	94–95	93–95 (54)
9	3-COMe	97.4	104–105	102–106 (55)
10	2-CHO	98.2	40–42	40–44 (56)
11	4-NO$_2$	97.6	143–146	144–147 (57)
12	2-NO$_2$-4-OMe	97.4	46–48	45–46 (58)
13	2-OH-5-Cl	98.5	135–138	136.2–138.1 (59)
14	4-COOH	93	186–188	187–189 (60)
15	2-Cl,5-NO$_2$	97.1	64–68	65–68 (61)
16	2-COOH	84	145–146	145 (62)
17	4-Br	97.4	60–62	60–61 (63)
18	4-COPh	80	121–123	120.1–122.2 (64)

^{a} Reaction conditions: nitroaromatic compounds (0.25 mmol), NaBH$_4$ (1 mmol), catalyst (10 mg), and solvent (5 μL), at 25 °C for 2 min. ^{b} The yields relate to the isolated product.

Table 9 Comparing mpg-C$_3$N$_4$@Pa@Ni with other catalysts in the reduction of nitroaromatic compounds

Entry	Catalyst	Temperature (°C)	Time (min)	Solvent (mL)	Yield (%)	Ref.
1	Ni–Fe$_3$O$_4$@Pectin ∼ PPA	25	15–45 min	H$_2$O (3)	80–98	65
2	RGO–Ni	120	16 min	H$_2$O (2)	72–99	66
3	Ag/MTA	25	1.5–26 h	EtOH	70–100	67
4	CuNPs	25	0.5–24 h	H$_2$O (5)	79–98	68
5	mpg-C$_3$N$_4$@Pa@Ni	25	2 min	H$_2$O (0.005)	80–98.6	Present work

published literature, shown in Table 9. The results of the assessment, which are presented in Table 9, indicate that the synthesized nanocomposite has demonstrated high efficiency as a catalyst in the target reaction. These outcomes suggest that mpg-C$_3$N$_4$@Pa@Ni has the potential to be a promising catalyst for nitroaromatic compound reduction, aligning with green
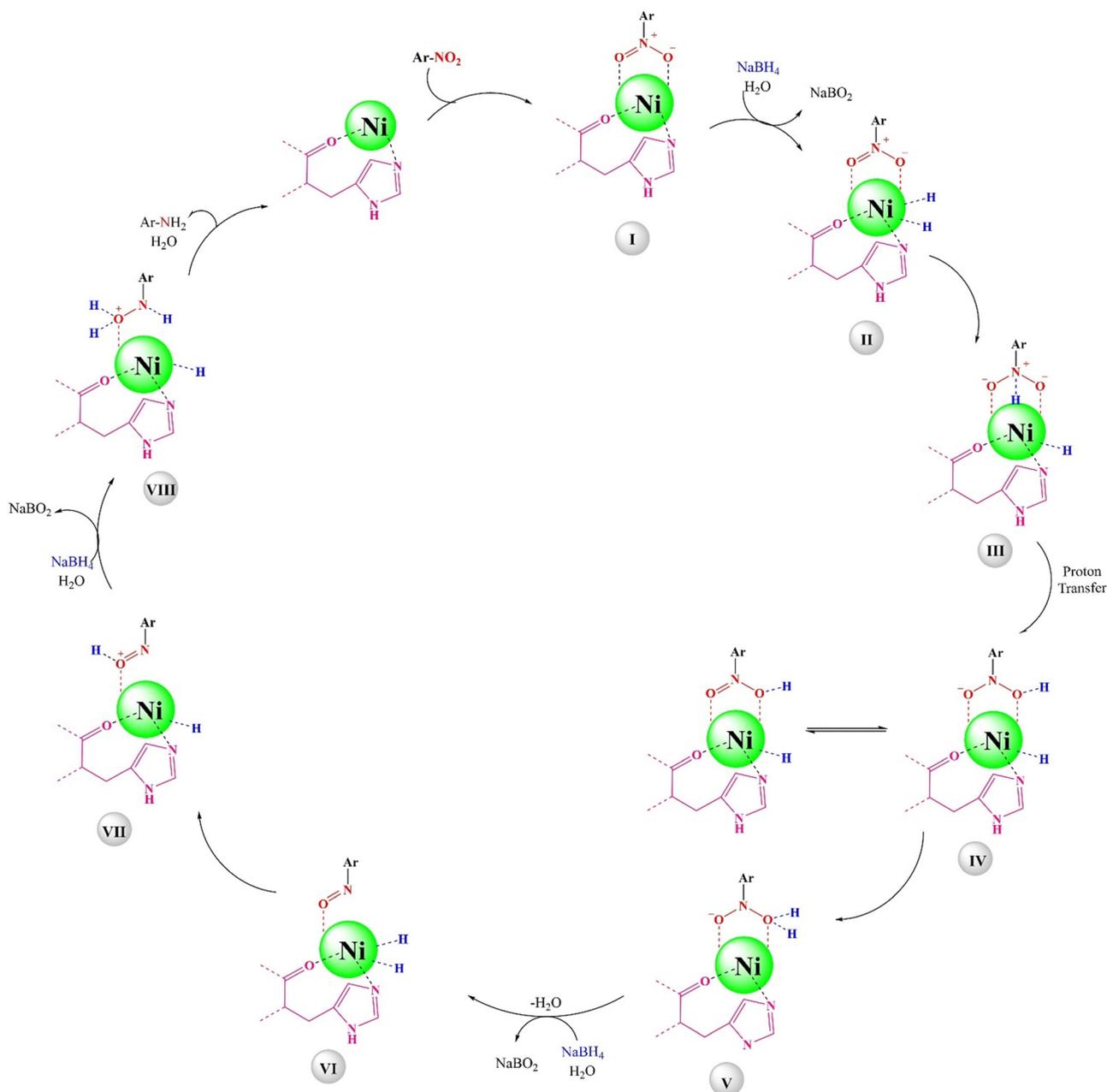

Fig. 13   The proposed mechanism for the reduction of nitroaromatic compounds.

chemistry principles due to its shorter reaction time and reduced solvent usage in comparison to other methods.

3.4. Catalytic mechanism

A schematic representation of the proposed mechanism for the reduction of nitroaromatic compounds using the mpg-C_3N_4@Pa@Ni nanocomposite is depicted in Fig. 13. The conversion of nitrobenzene to aniline by the mpg-C_3N_4@Pa@Ni nanocomposite involves several steps. Step (I): nitrobenzene (Ar-NO_2) is adsorbed onto the Ni metal surfaces of the nanocomposite, which serves as the primary active site for the reduction process. The Ni nanoparticles play a crucial role by providing the surface necessary for the adsorption and activation of nitrobenzene. Step (II): $NaBH_4$ reacts with water to produce hydride ions (H^-), which are then adsorbed onto the surface of the Ni metal. Step (III): these hydride ions interact with the positively charged nitrogen atom of the nitro group in nitrobenzene, initiating the reduction process. Step (IV): a hydrogen shift occurs, wherein the hydrogen atom attached to the nitrogen transfers to one of the oxygens of the nitro group, resulting in resonance stabilization and forming a nitrogen-oxygen double bond. Step (V): another hydride ion attaches to the oxygen of the nitro group, converting it into a good leaving group ($-H_2O^+$) that subsequently departs from the molecule. Step (VI): the departure of the leaving group results in forming a nitroso intermediate. Step (VII): a hydride ion on the Ni surface subsequently interacts with the oxygen of the nitroso

intermediate, facilitating its reduction. Step (VIII): another hydride ion then interacts with the nitroso intermediate, creating another suitable leaving group ($-H_2O^+$). Simultaneously, a hydride ion interacts with the nitrogen of the nitroso group. The elimination of the leaving group and the release of another water molecule leads to the formation of an amine group, resulting in the release of aniline from the catalyst surface. This mechanism underscores the efficiency of the mpg-C_3N_4@Pa@Ni nanocomposite as a catalyst in reducing nitrobenzene to aniline. Additionally, the role of mpg-C_3N_4 and papain in the nanocomposite should not be overlooked. The mesoporous structure of mpg-C_3N_4 enhances the dispersion of Ni nanoparticles, increasing the available surface area for catalytic reactions. Papain, on the other hand, contributes to the structural stability and coordination, further improving the catalytic performance of the nanocomposite. The combined effects of these components make the mpg-C_3N_4@Pa@Ni an efficient and robust catalyst for nitroaromatic reduction. Moreover, the nitroso intermediate (MP: 132–133 °C)[69] was synthesized, and the reaction proceeded from step (VI) to validate the mechanism.

3.5. Reusability

The process of catalyst recycling is highly significant in green chemistry and environmental preservation, as it allows for the development of catalysts that are efficient, durable, and sustainable. This parameter is also essential in practical
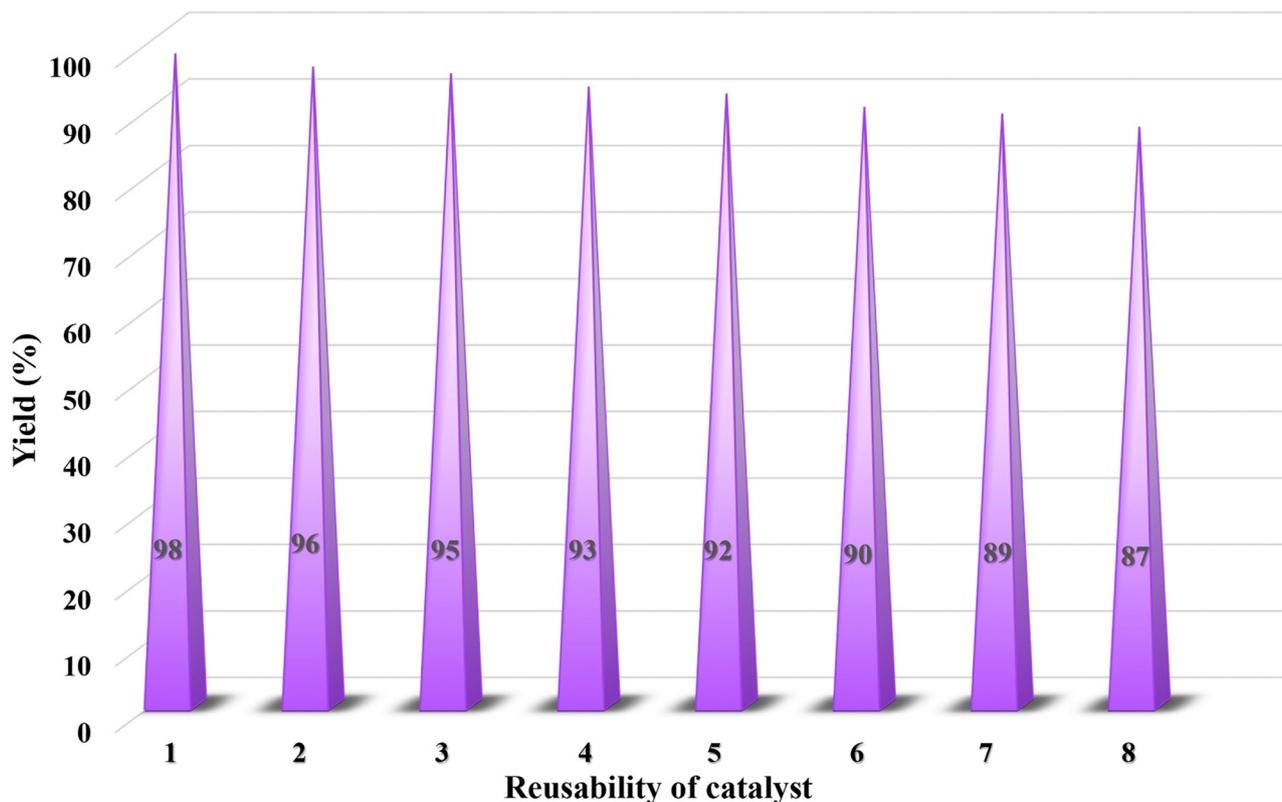

Fig. 14 Recycling ability of the mpg-C_3N_4@Pa@Ni catalyst in the reduction of nitrobenzene.

applications, as it aids researchers in identifying catalysts capable of enduring multiple reuse cycles. To ensure a thorough investigation, the quantities of all reaction components were doubled, which negligible losses during the separation of the catalyst after each cycle, as demonstrated in Fig. 14. This doubling of components was implemented to enhance experimental accuracy and to achieve the desired results with maximum efficiency. Initially, the catalyst's recyclability was tested up to five cycles and subsequently extended to eight cycles to assess its performance over a longer reuse period. During this extended evaluation, a slight reduction in efficiency was observed from 92% at cycle five to 87% at cycle eight indicating that the catalytic activity gradually decreases when the catalyst is used beyond five cycles. The study of the mpg-C$_3$N$_4$@Pa@Ni nanocomposite revealed that the content of the nanocomposite before washing was 20 mg, while after eight reuses, it decreased to 19.2 mg. This indicates a minimal reduction in reaction efficiency, which can be attributed to the occupation of the catalyst's active sites. The study revealed that the catalyst was effective and could be reused multiple times with minimal loss of efficiency. Upon conducting a comparative analysis of the FT-IR and EDS spectra of the recovered catalyst with the original catalysts depicted in Fig. S1 and S2 (ESI†), respectively, it can be inferred that the functional groups and elements have been retained. The analysis also indicates that the catalyst exhibits excellent performance even after undergoing eight cycles of use. These findings demonstrate that the catalyst maintains exceptional performance and structural integrity even after eight reuse cycles, underscoring its robustness and suitability for multiple applications with minimal efficiency loss.

4. Conclusion

In this research, the mpg-C$_3$N$_4$@Pa@Ni nanocomposite, a highly effective catalyst for reducing harmful nitroaromatic compounds, was synthesized through a four-step process. Evidence-based reduction of harmful nitroaromatic compounds with several solvent-free methods such as using a mortar and pestle, ball mill, microwave, and magnetic stirrer were evaluated to identify the most effective way to perform this reaction. In the course of the investigation, it was discovered that all the methods under scrutiny achieved 98.6% efficiency. The results showed that the magnetic stirrer method was the most efficient, consumed the least amount of energy, and produced the desired outcome in the shortest time. Also, using the magnetic stirrer method, the recovery of the mpg-C$_3$N$_4$@Pa@Ni nanocomposite was investigated up to 8 cycles, and exhibited impressive performance. Moreover, even after eight recovery cycles, this nanocomposite demonstrated a significant yield for catalytic reactions. Using the solvent-less method as a green method and the absence of the need for high temperature, large amounts of solvent, and high energy made this method highly useful in reducing harmful nitroaromatic compounds. The results obtained from the study were deemed acceptable, indicating the potential of this nanocomposite to be applied in various industries to reduce harmful nitroaromatic compounds.

Author contributions

Hossein Ghafuri was responsible for the conceptualization and supervision. Fatemeh Eshrati performed the experiments, writing of the original draft of the manuscript, and data analysis. Haniyeh Dogari analyzed data. Peyman Hanifehnejad assisted in data analysis, the original draft of the manuscript, and the methodology.

Data availability

The data that support the findings of this study are available from the corresponding author, Hossein Ghafuri, upon reasonable request. The data include raw experimental data, analyzed data, and supporting information. Additionally, any supplementary information related to this study is included in the supplementary materials section of this manuscript. For any additional information or data requests, please contact ghafuri@iust.ac.ir.

Conflicts of interest

There are no conflicts to declare.

Acknowledgements

References

1 N. T. Dung, P. T. H. Hanh, V. D. Thao, N. T. Thuy, D. T. M. Thanh, N. T. Phuong, K.-Y. A. Lin and N. N. Huy, *Environ. Sci.: Water Res. Technol.*, 2023, **9**, 221–234.

2 F. Besharat, F. Ahmadpoor, Z. Nezafat, M. Nasrollahzadeh, N. R. Manwar, P. Fornasiero and M. B. Gawande, *ACS Catal.*, 2022, **12**, 5605–5660.

3 A. Rashidizadeh, H. Ghafuri, N. Goodarzi and N. Azizi, *Solid State Sci.*, 2020, **109**, 106427.

4 H. Ghafuri, Z. Tajik, N. Ghanbari and P. Hanifehnejad, *Sci. Rep.*, 2021, **11**, 19792.

5 Y. Cao, G. Zhou, X. Chen, Q. Qiao, C. Zhao, X. Sun, X. Zhong, G. Zhuang, S. Deng and Z. Wei, *J. Mater. Chem. A*, 2020, **8**, 124–137.

6 S. Samanta and R. Srivastava, *Mater. Adv.*, 2020, **1**, 1506–1545.

7 M. Singh, A. Kumar and V. Krishnan, *Mater. Adv.*, 2020, **1**, 1262–1272.

8 V. SP, S. DS and A. B. Shbil, *Adv. Mater. Process. Technol.*, 2024, 1–16.

9 H. Ghafuri, A. Rashidizadeh, M. G. Gorab and G. Jafari, *Sci. Rep.*, 2022, **12**, 2331.

10 A. Rashidizadeh, H. Ghafuri, H. R. Esmaili Zand and N. Goodarzi, *ACS Omega*, 2019, **4**, 12544–12554.

11 H. Li, L. Wang, Y. Liu, J. Lei and J. Zhang, *Res. Chem. Intermed.*, 2016, **42**, 3979–3998.

12 C. Dai, Z. Feng, Q. Hu, J. Qiu, J. You, R. Guo and H. Zhang, *Mater. Sci. Semicond. Process.*, 2023, **167**, 107807.

13 B. A. Babalola, A. I. Akinwande, A. A. Otunba, G. E. Adebami, O. Babalola and C. Nwufo, *Arabian J. Chem.*, 2024, **17**, 105369.

14 M. Akhgari, E. Mosaffa, H. Dogari, N. A. Ramsheh, H. Ghafuri and A. Banerjee, *Environ. Sci.: Water Res. Technol.*, 2023, **9**, 2112–2127.

15 W. Li, X.-s Chu, F. Wang, Y.-y Dang, X.-y Liu, X.-c Wang and C.-y Wang, *Appl. Catal., B*, 2021, **288**, 120034.

16 M. A. D. Fard, H. Ghafuri and A. Rashidizadeh, *Microporous Mesoporous Mater.*, 2019, **274**, 83–93.

17 L. K. Mueller, M. Ågerstrand, T. Backhaus, M. Diamond, W. R. Erdelen, D. Evers, K. J. Groh, M. Scheringer, G. Sigmund and Z. Wang, *Environ. Sci.: Adv.*, 2023, **2**, 151–161.

18 J.-P. Zou, D.-D. Wu, J. Luo, Q.-J. Xing, X.-B. Luo, W.-H. Dong, S.-L. Luo, H.-M. Du and S. L. Suib, *ACS Catal.*, 2016, **6**, 6861–6867.

19 D. Zhang, Y. Li, A. Sun, S. Tong, G. Su, X. Jiang, J. Li, W. Han, X. Sun and L. Wang, *Sci. Total Environ.*, 2019, **694**, 133701.

20 H. Wang, H.-P. Zhao and L. Zhu, *Environ. Sci. Technol.*, 2020, **54**, 8760–8769.

21 S. Doherty, J. G. Knight, T. Backhouse, R. J. Summers, E. Abood, W. Simpson, W. Paget, R. A. Bourne, T. W. Chamberlain and R. Stones, *ACS Catal.*, 2019, **9**, 4777–4791.

22 Q. Zhang, J. Bu, J. Wang, C. Sun, D. Zhao, G. Sheng, X. Xie, M. Sun and L. Yu, *ACS Catal.*, 2020, **10**, 10350–10363.

23 V. A. R. Villegas, J. I. D. L. Ramírez, E. H. Guevara, S. P. Sicairos, L. A. H. Ayala and B. L. Sanchez, *J. Saudi Chem. Soc.*, 2020, **24**, 223–235.

24 L. R. Shultz, B. McCullough, W. J. Newsome, H. Ali, T. E. Shaw, K. O. Davis, F. J. Uribe-Romo, M. Baudelet and T. Jurca, *Molecules*, 2019, **25**, 89.

25 A. Gawel, S. Sühnholz, A. Georgi, F.-D. Kopinke and K. Mackenzie, *J. Hazard. Mater.*, 2023, **459**, 132125.

26 S. Payamifar and A. Poursattar Marjani, *Appl. Organomet. Chem.*, 2023, **37**, e7287.

27 D. Cheng, Y. Tan, R. Ma, H. Ding, W. Liao, K. He, R. Sun, H. Ni and F. He, *Environ. Sci. Technol.*, 2023, **57**, 19827–19837.

28 S. Wang, J. Zhu, T. Li, F. Ge, Z. Zhang, R. Zhu, H. Xie and Y. Xu, *Environ. Sci. Technol.*, 2022, **56**, 7924–7934.

29 G. Pandey, N. Singh, N. Rajput, M. K. Saini, S. Kothari, J. Prasad, N. P. Lamba and M. S. Chauhan, *Sci. Rep.*, 2024, **14**, 2077.

30 M. Kashihara and Y. Nakao, *Acc. Chem. Res.*, 2021, **54**, 2928–2935.

31 F. Ferretti, D. R. Ramadan and F. Ragaini, *ChemCatChem*, 2019, **11**, 4450–4488.

32 A. Saha and B. Ranu, *J. Org. Chem.*, 2008, **73**, 6867–6870.

33 S. M. Kelly and B. H. Lipshutz, *Org. Lett.*, 2014, **16**, 98–101.

34 J. Wen, J. Xie, X. Chen and X. Li, *Appl. Surf. Sci.*, 2017, **391**, 72–123.

35 H. Zhao and C.-H. Kong, *Chem. Eng. J.*, 2018, **339**, 424–431.

36 S. P. Swain, N. Prasad, L. Reddy, G. Subrahmanyam and S. Mohanty, *ChemistrySelect*, 2021, **6**, 1088–1092.

37 A. Porcheddu, E. Colacino, L. De Luca and F. Delogu, *ACS Catal.*, 2020, **10**, 8344–8394.

38 J. D. Jiménez, L. E. Betancourt, M. Danielis, H. Zhang, F. Zhang, I. Orozco, W. Xu, J. Llorca, P. Liu and A. Trovarelli, *ACS Catal.*, 2022, **12**, 12809–12822.

39 L. Gong, L. Qiu, X. Xing, J. Zhu, M. Lu, F. Dong, Y. Yu and W. Yu, *Sci. Total Environ.*, 2024, **912**, 169161.

40 H. Ahmad and M. K. Hossain, *Mater. Adv.*, 2022, **3**, 859–887.

41 M. Cronau, M. Szabo and B. Roling, *Mater. Adv.*, 2021, **2**, 7842–7845.

42 S. Mancillas-Salas, P. Hernández-Rodríguez, A. Reynosa-Martínez and E. López-Honorato, *MRS Adv.*, 2020, **5**, 3133–3140.

43 Z. Jahani, E. Mosaffa, M. Oroujzadeh and H. Ghafuri, *Polym. Adv. Technol.*, 2023, **34**, 3803–3817.

44 S. Elavarasan, B. Baskar, C. Senthil, P. Bhanja, A. Bhaumik, P. Selvam and M. Sasidharan, *RSC Adv.*, 2016, **6**, 49376–49386.

45 M. Tasbihi, F. Fresno, I. Alvarez-Prada, A. Acharjya, A. Thomas, L. Escriche, N. Romero, X. Sala and J. García-Antón, *J. CO2 Util.*, 2021, **50**, 101574.

46 Y. Sahoo, Y. He, M. Swihart, S. Wang, H. Luo, E. Furlani and P. Prasad, *J. Appl. Phys.*, 2005, **98**, 5.

47 W.-J. Niu, J.-Z. He, Y.-P. Wang, Q.-Q. Sun, W.-W. Liu, L.-Y. Zhang, M.-C. Liu, M.-J. Liu and Y.-L. Chueh, *Nanoscale*, 2020, **12**, 19644–19654.

48 Q. Lin, L. Li, S. Liang, M. Liu, J. Bi and L. Wu, *Appl. Catal., B*, 2015, **163**, 135–142.

49 R. Taheri-Ledari, M. Saeidirad, F. S. Qazi, A. Fazeli, A. Maleki and A. E. Shalan, *RSC Adv.*, 2021, **11**, 25284–25295.

50 A. Ghatak and S. Bhar, *Synth. Commun.*, 2022, **52**, 368–379.

51 S. B. Lee, S. Chun, S. H. Choi, J. Hong, D.-C. Oh and S. Hong, *J. Org. Chem.*, 2023, **88**, 1234–1245.

52 M. Gholinejad, M. Shojafar, J. M. Sansano, V. N. Mikhaylov, I. A. Balova and R. Khezri, *J. Organomet. Chem.*, 2022, **970**, 122359.

53 V. Kandathil, T. S. Koley, K. Manjunatha, R. B. Dateer, R. S. Keri, B. Sasidhar, S. A. Patil and S. A. Patil, *Inorg. Chim. Acta*, 2018, **478**, 195–210.

54 D. Peña-Solórzano, M. Scholler, G. N. Bernhardt, A. Buschauer, B. König and C. Ochoa-Puentes, *ACS Med. Chem. Lett.*, 2018, **9**, 854–859.

55 M. Jang, T. Lim, B. Y. Park and M. S. Han, *J. Org. Chem.*, 2022, **87**, 910–919.

56 P. K. Lakshmi, S. V. Markandeya, C. Sridhar and N. Annapurna, *Synth. Commun.*, 2022, **52**, 1628–1634.

57 S. Fekri, Y. Mansoori and A. Bezaatpour, *J. Organomet. Chem.*, 2023, **993**, 122724.

58 S. S. Mahajan and R. G. Nandre, *Mater. Adv.*, 2006, **37**(46), DOI: **10.1002/chin.200646019.**

59 Z. Hu, Y. Ai, L. Liu, J. Zhou, G. Zhang, H. Liu, X. Liu, Z. Liu, J. Hu and Hb Sun, *Adv. Synth. Catal.*, 2019, **361**, 3146–3154.

60 M. Guidetti, R. Hilfiker, M. Kuentz, A. Bauer-Brandl and F. Blatter, *Cryst. Growth Des.*, 2022, **23**, 842–852.

61 M. Moradi, N. Rastakhiz, M. Ghaedi and R. Zhiani, *Catal. Lett.*, 2021, **151**, 1653–1662.

62 P. Karthikeyan, R. V. Jagadeesh, Y. Sree Sandhya, P. Puttaswamy, P. Nithya, S. Senthil Kumar and P. Bhagat, *Appl. Organomet. Chem.*, 2011, **25**, 34–46.

63 N. R. Lee, A. A. Bikovtseva, M. Cortes-Clerget, F. Gallou and B. H. Lipshutz, *Org. Lett.*, 2017, **19**, 6518–6521.

64 A. Sumita, Y. Otani and T. Ohwada, *Chem. Commun.*, 2017, **53**, 1482–1485.

65 P. Ghamari Kargar, A. Ravanjamjah and G. Bagherzade, *J. Chin. Chem. Soc.*, 2021, **68**, 1916–1933.

66 M. Karthik and P. Suresh, *ChemistrySelect*, 2017, **2**, 6916–6928.

67 D. Andreou, D. Iordanidou, I. Tamiolakis, G. S. Armatas and I. N. Lykakis, *Nanomaterials*, 2016, **6**, 54.

68 R. Rai and D. K. Chand, *J. Chem. Sci.*, 2021, **133**, 87.

69 A. Hashidoko, T. Kitanosono, Y. Yamashita and S. Kobayashi, *Org. Lett.*, 2024, **26**, 5517–5521.